Espectroscopia de Fotoelétrons Excitados por Raios X

Parte II

Professor Doutor

Ubirajara Pereira Rodrigues Filho

Estudo de Casos

Compostos Inorgânicos

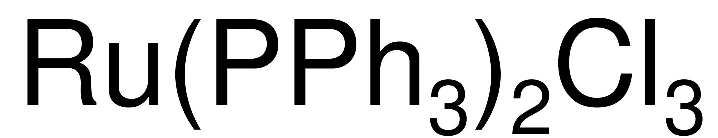
$Ru(PPh_3)_2Cl_3$

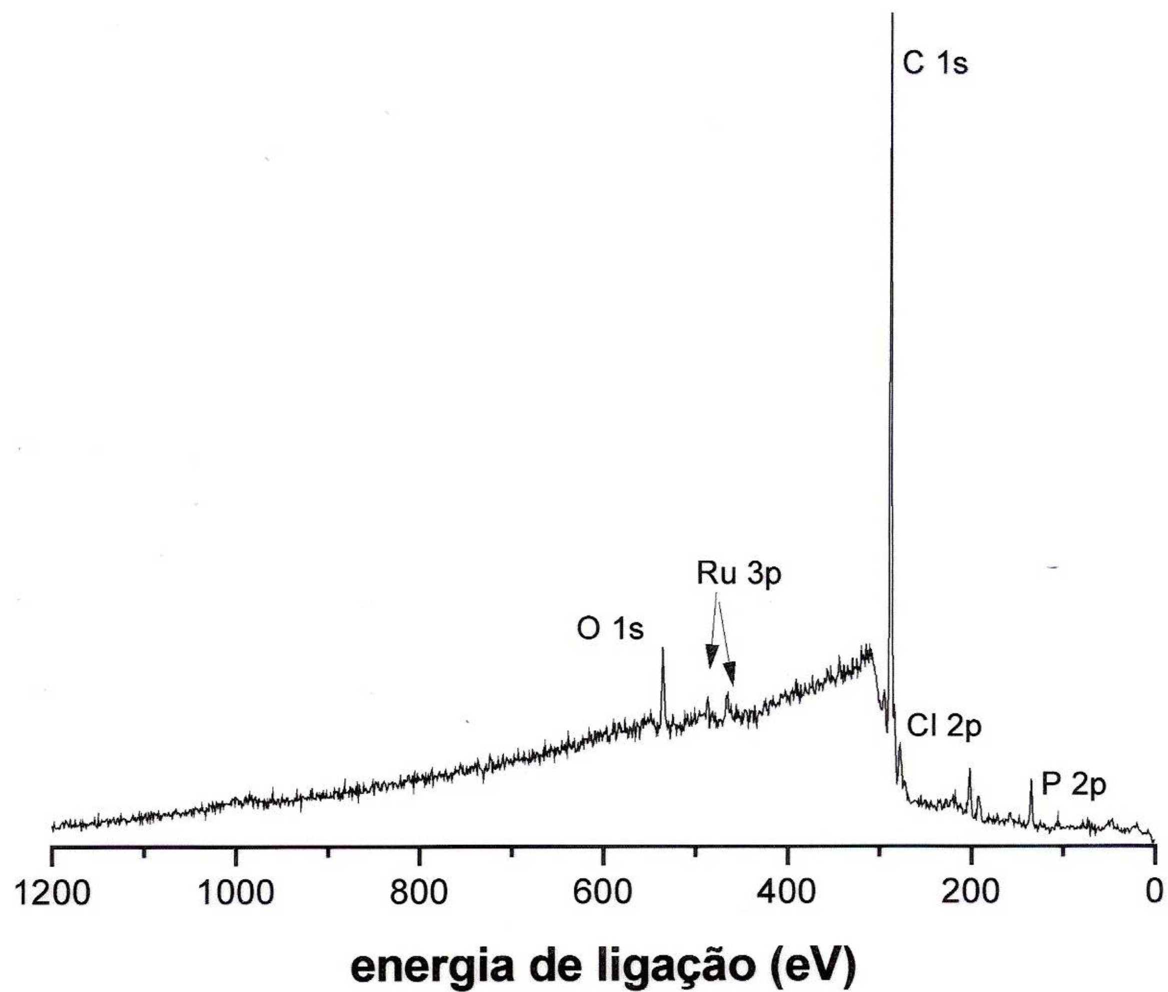

Figura 7: espectro geral do complexo $[Ru(PPh_3)_3Cl_2]$ obtido por XPS.

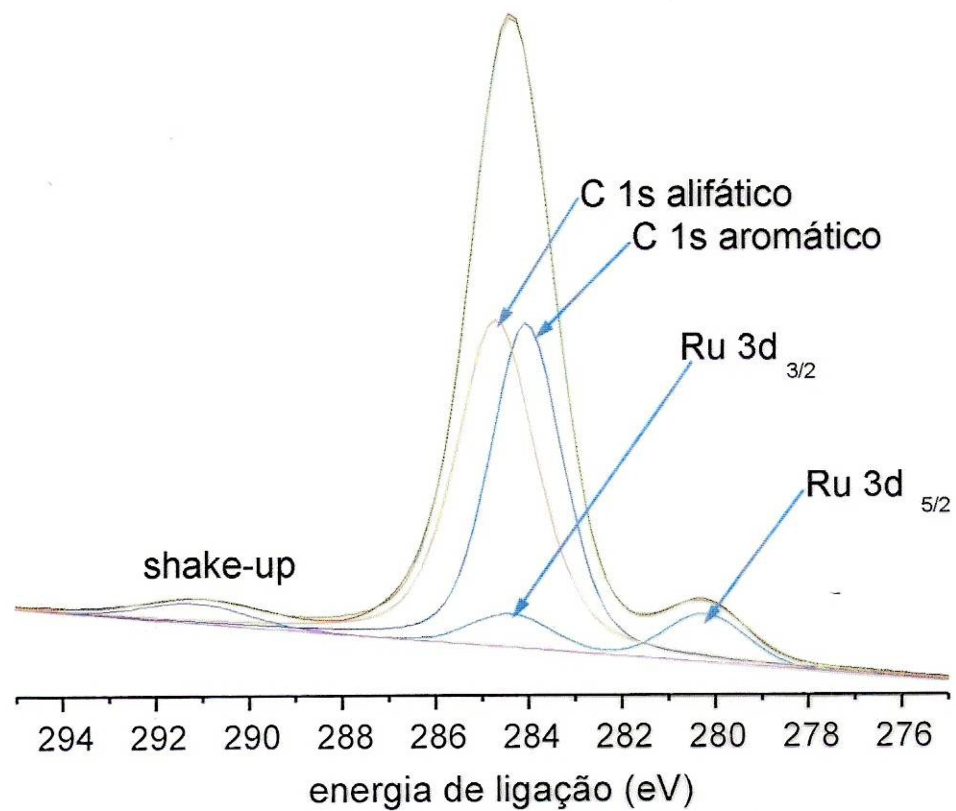

Figura 2: Espectro de Fotoemissão Excitada por Raios-X na região do C 1s e Ru 3d para o complexo $Ru(PPh_3)_3Cl_2]$.

Magalhães, JL; Rodrigues-Filho, UP; de Castro, SC; dados não publicados.

C1s em Cianoferratos

Ao oxidar o $Fe^{II}(CN)_6^{4-}$ a $Fe^{III}(CN)_6^{3-}$ dois efeitos atuam juntos para aumentar o valor da E_L(C1s) do cianeto:

a) Aumento do estado de oxidação do metal ligado ao N leva a um aumento da eletronegatividade do Fe e conseqüente maior efeito sacador de elétrons do Fe sobre o C e o N do cianto;
b) Oxidação leva a desapareciemtno da retrodoação que servia para aumentar a densidade eletrônica sobre o C e o N do cianeto.

Energia de Ligação

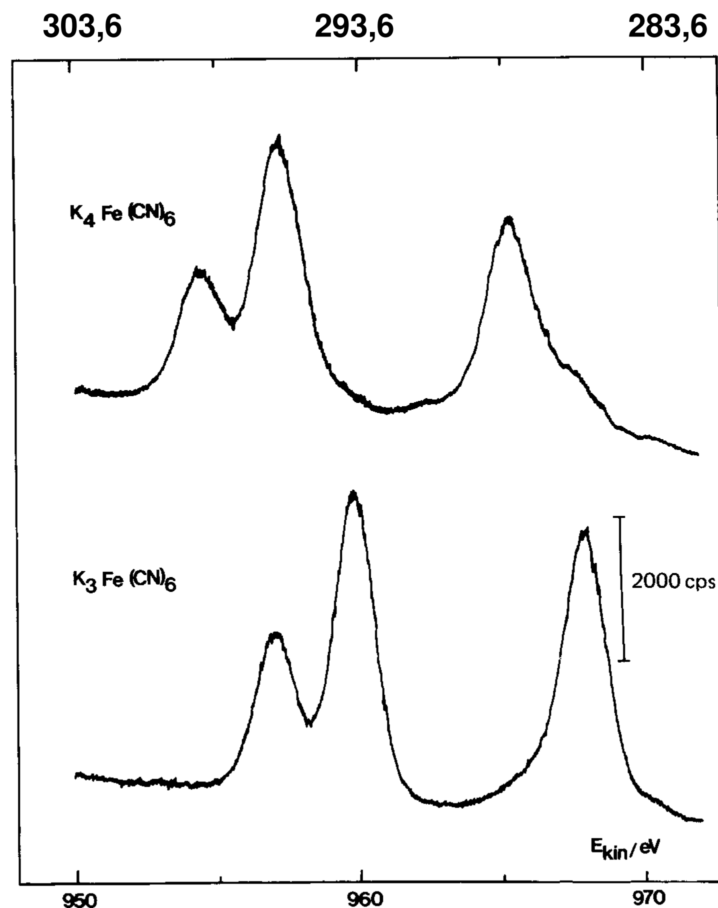

Fig. 2. Examples of spectra to show the difference in the C_{1s} peak form, indicating satellites in the upper case. The spectra are uncorrected for charging effects.

hυ=1253,6 eV

Ragnar Larsson and Börje Folkesson

Chemica Scripta. Vol. 19, 27–30, 1982

XPS de Cianoferratos

Compound	E_b eV	
	N_{1s}	C_{1s}
$K_4V(CN)_6$	398.5	284.2
$K_4Mn(CN)_6$	397.0	283.6
$K_4Fe(CN)_6$	397.0	284.1
$K_3Cr(CN)_6$	397.8	283.9
$K_3Mn(CN)_6$	397.5	284.3
$K_3Fe(CN)_6$	397.4	284.2
$K_3Co(CN)_6$	397.3	283.8
$K_2Ni(CN)_4$	397.4	284.1
$K_2Pd(CN)_4$	397.6	284.2
$K_2Pt(CN)_4$	397.1	284.0
$K\ Au(CN)_4$	397.6	284.1

XPS e Estado de Estado de Oxidação

Fluoretos de Xe

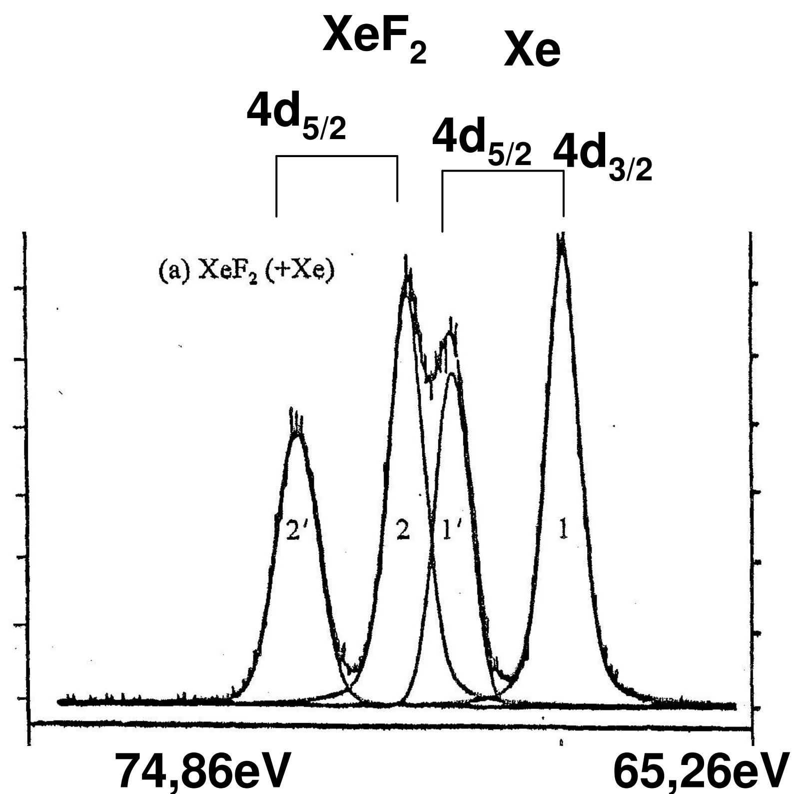

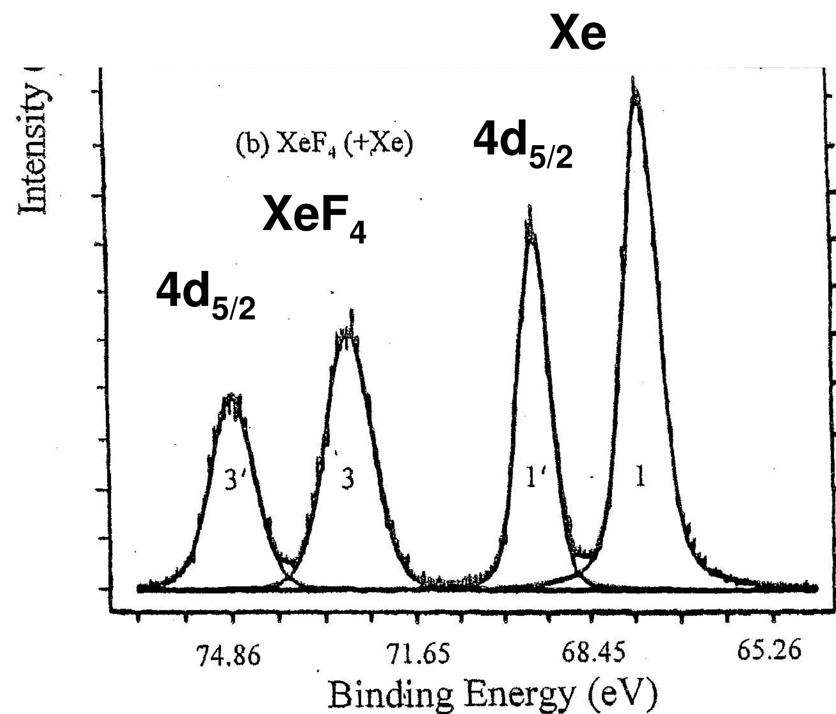

11. The Xe $4d_{5/2}$ and $4d_{3/2}$ photoelectron spectra taken at a total r with a monochromatized Al Kα source. a) XeF_2 (2 and 2′) with Xe (3 and 3′) and Xe (1 and 1′).[38]

XPS

Ligante em Ponte vs Ligante Terminal

XPS e Caracterização do Ligante

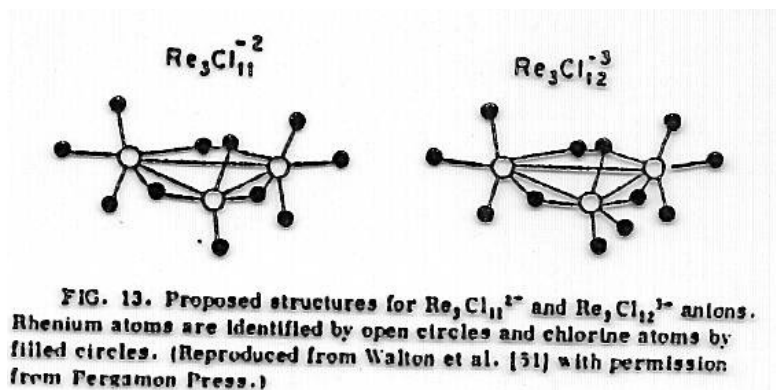

FIG. 13. Proposed structures for $Re_3Cl_{11}^{2-}$ and $Re_3Cl_{12}^{3-}$ anions. Rhenium atoms are identified by open circles and chlorine atoms by filled circles. (Reproduced from Walton et al. [51] with permission from Pergamon Press.)

TABLE 11

Cl 2p Binding Energies (eV) in Some Rhenium Halides [51]

	Cl $2p_{3/2}$	
Compound	Cl_b	Cl_t
$Cs_3Re_3Cl_{12}$	199.4	197.9
$[AcrH]_3Re_3Cl_{12}$	199.0	197.8
$[pyH]_2Re_3Cl_{11}$	199.2	197.9
$[\alpha\text{-picH}]_2Re_3Cl_{11}$	199.0	197.9
$[bipyH]_2Re_3Cl_{11}$	199.1	198.0
$(bipyH_2)Re_3Cl_{11}$	199.0	198.0
$\{[AcrH]_2Re_3Cl_8\}_n$	198.7	197.6

Polímeros

XPS of Poly(ethylene terephthalate)

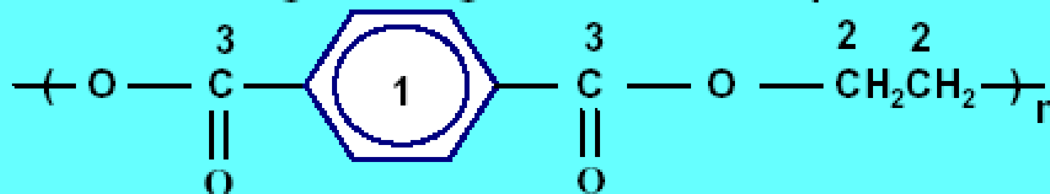

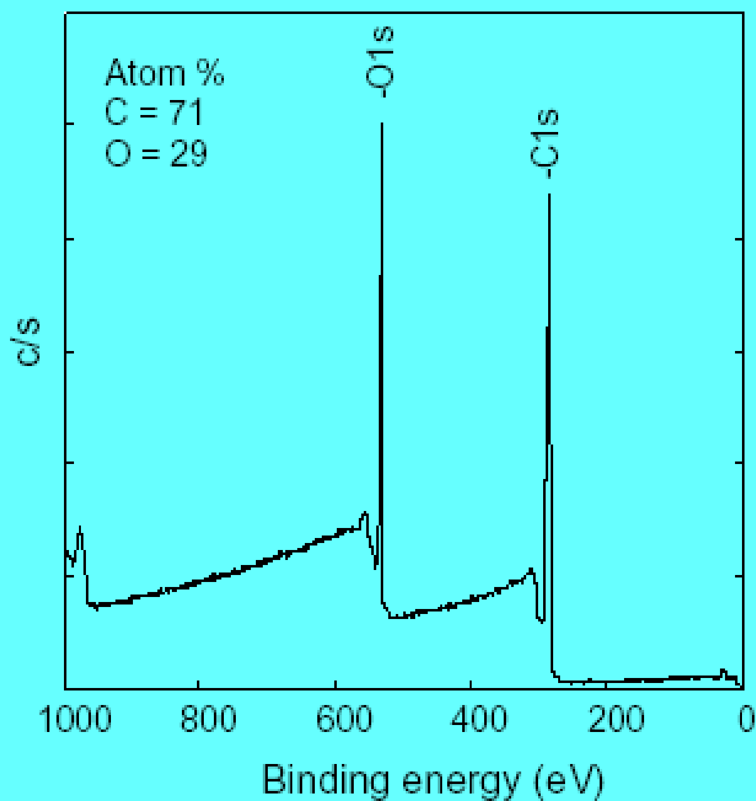

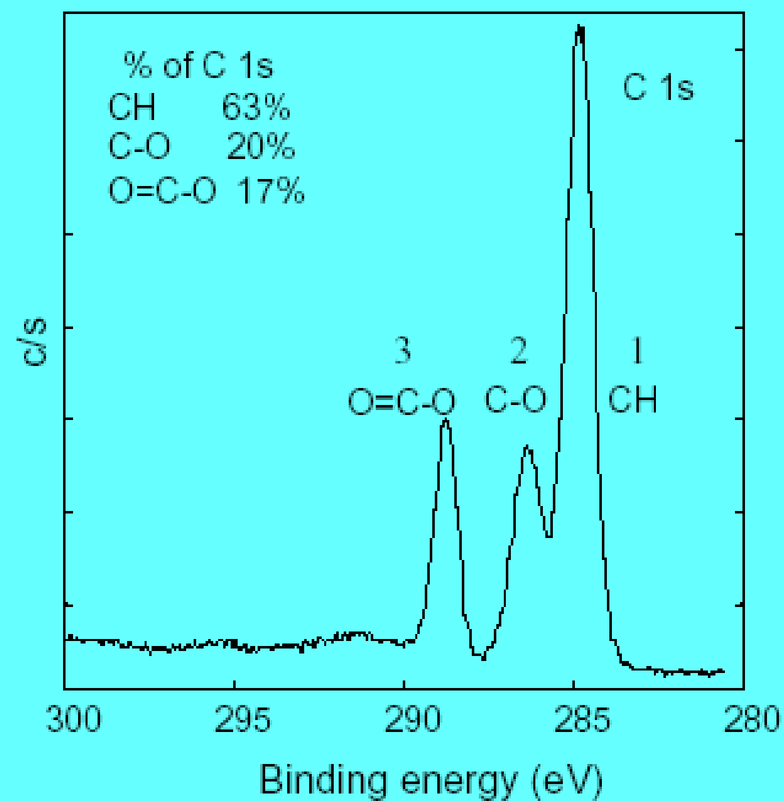

Blendas Poliméricas

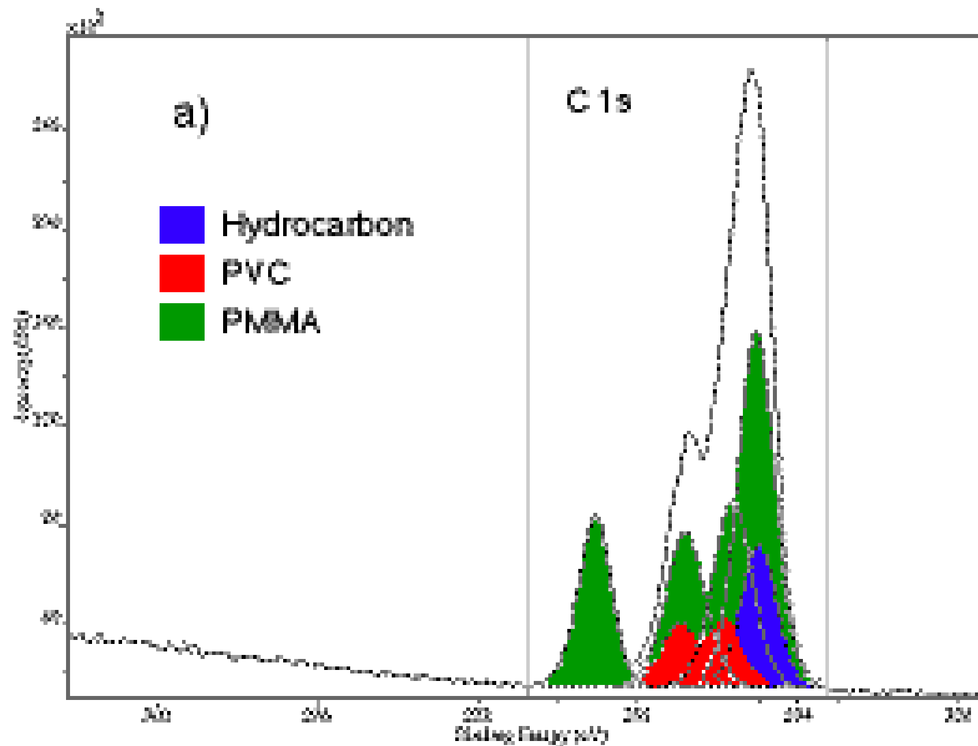

Espectro XP C1s de blenda de PVC e PMMA

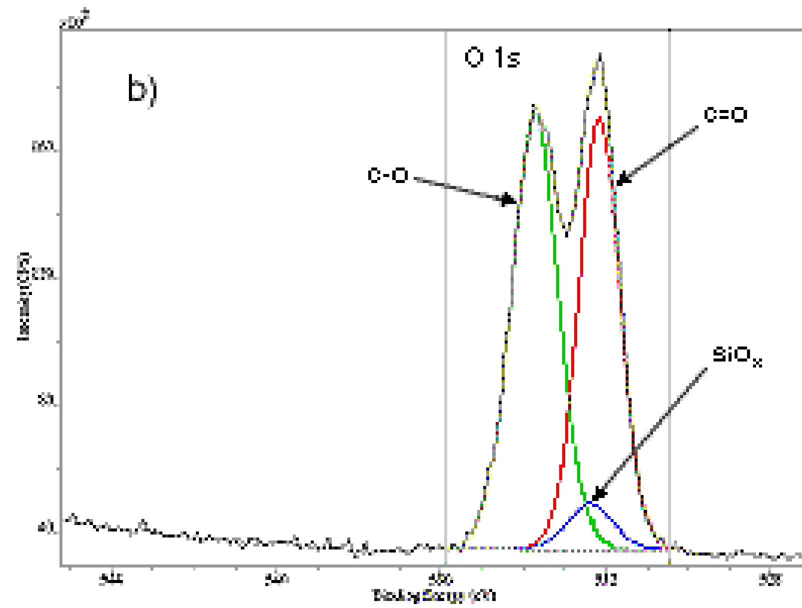
b)
O 1s
C-O
C=O
SiO_x

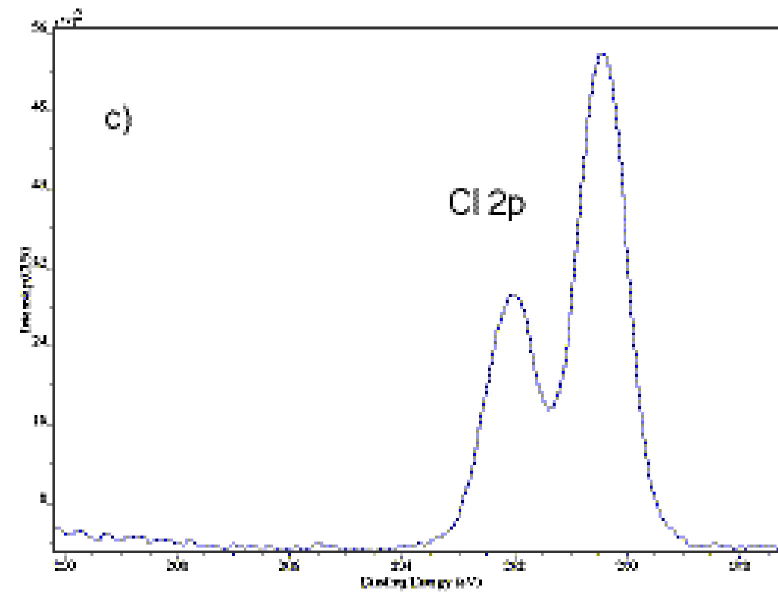
c)
Cl 2p

Cl2p

O1s

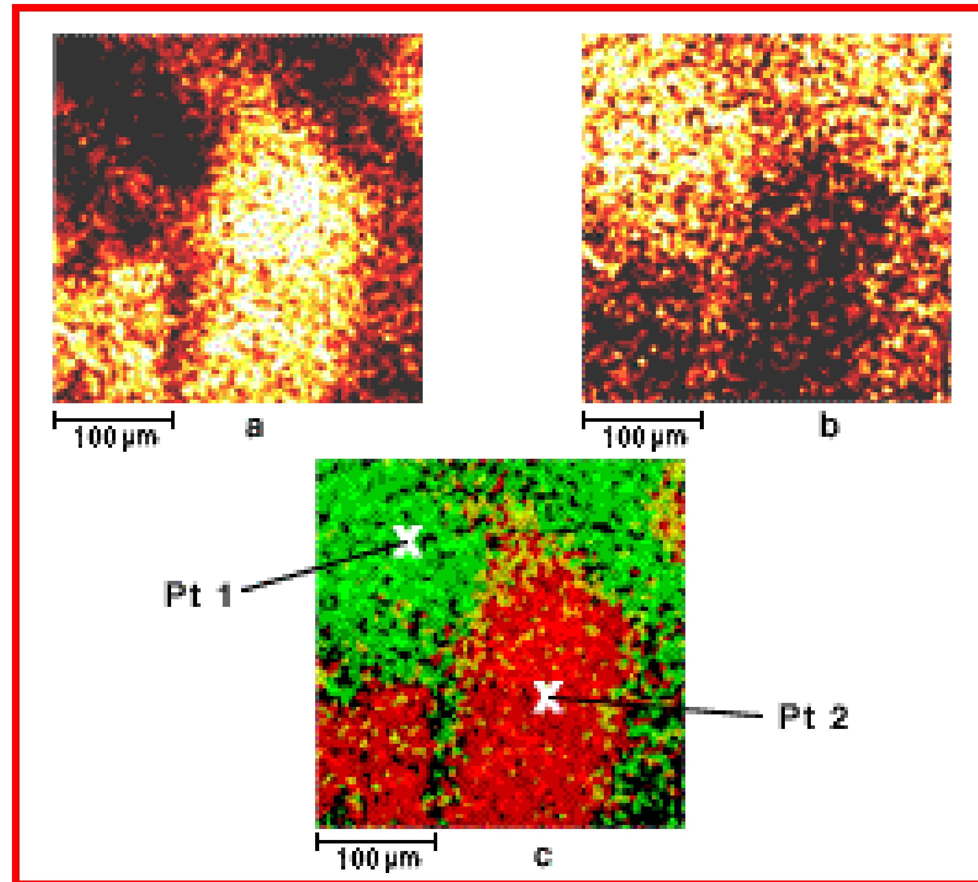

Distribuição dos dois polímeros da blenda seguida pelas imagens dos picos de fotoemissão Cl2p e O1s, a e b respectivamente. A imagem **no canto inferior mostra a superposição das duas regiões, Cl2p em vermelho.**

Adesivos
Resinas Epóxido

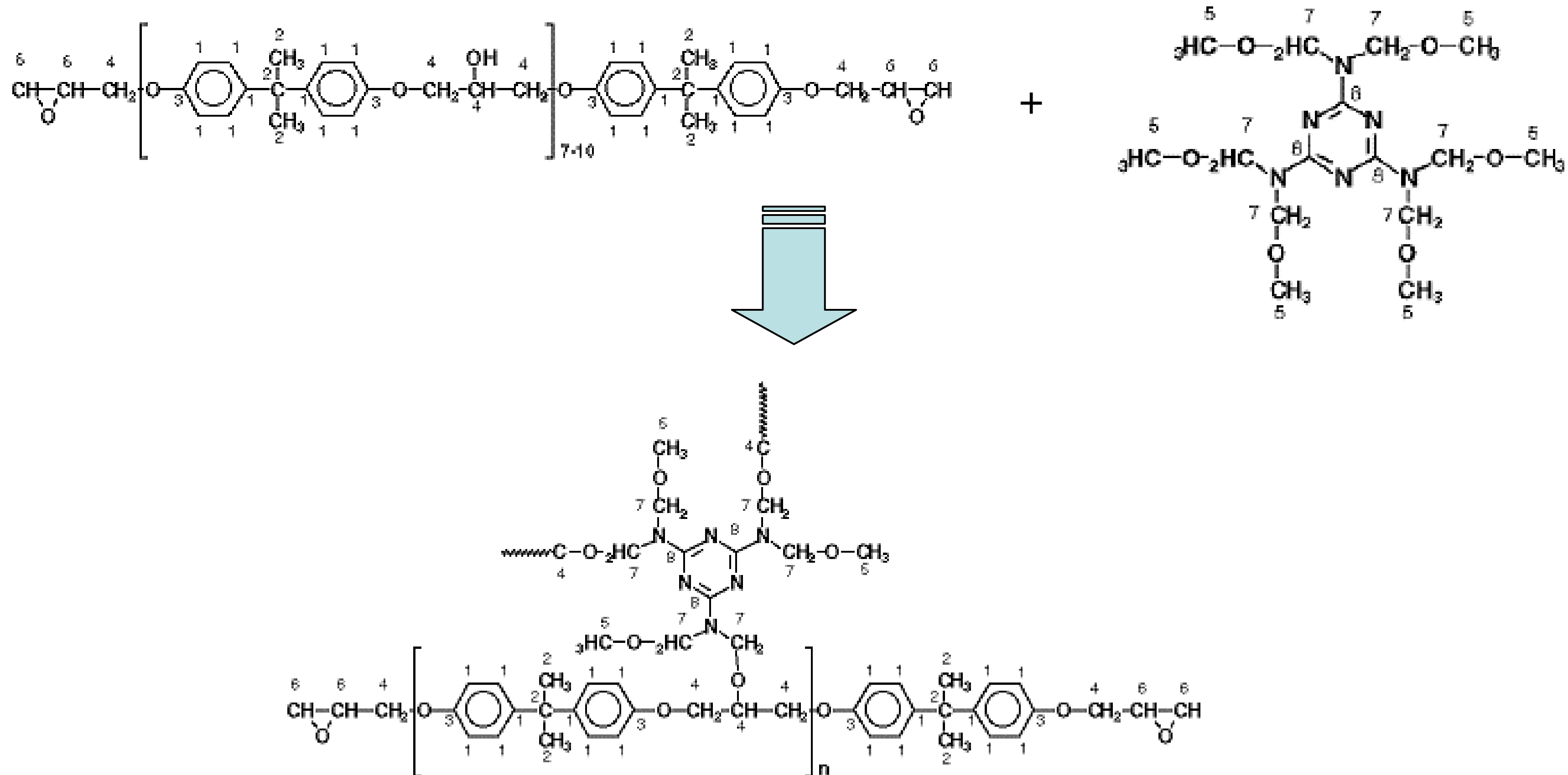

S.R. Leadley[1], J. F. Watts [1], C.J. Blomfield[2] and B. Tielsch[2]

Adesivos
Resinas Epóxido

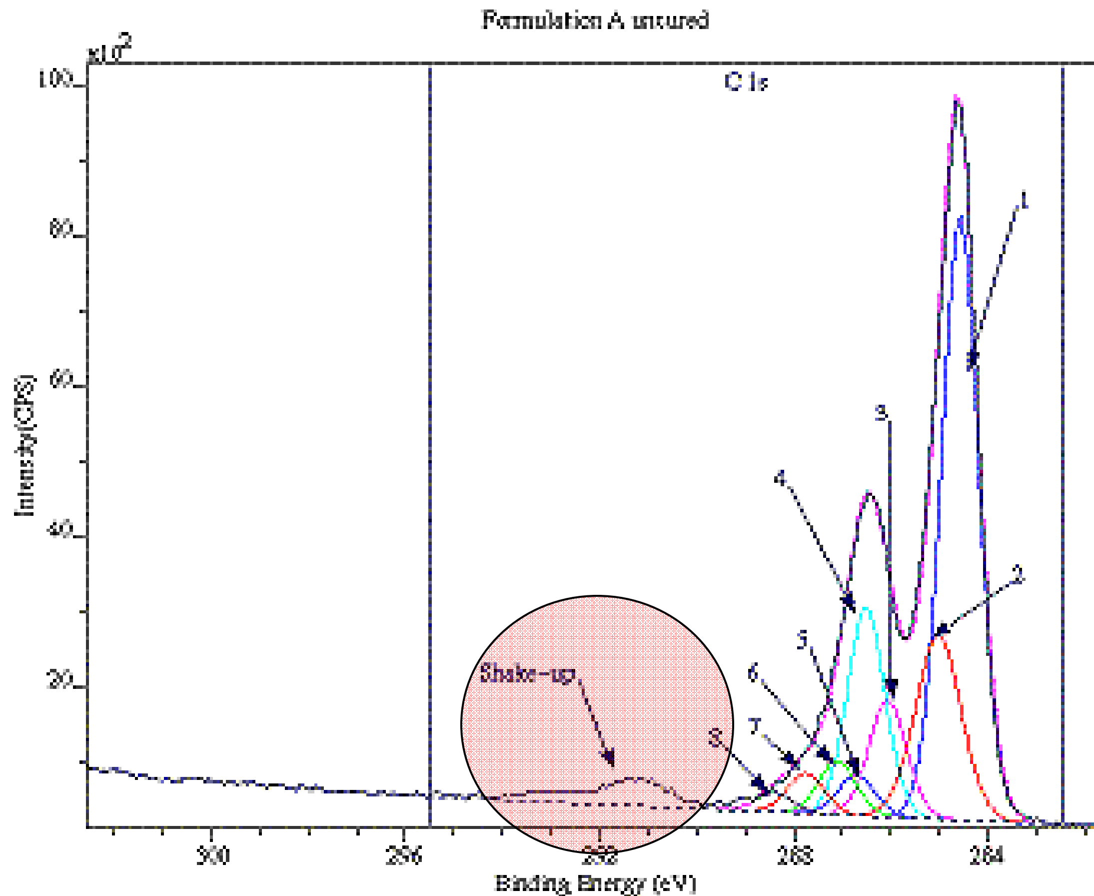

Espectro XP C1s antes da cura. Picos 1 a 6 associados ao epóxido e 5 a 8 associados à melanina.

Adesivos
Resinas Epóxido Adesivos
Resinas Epóxido

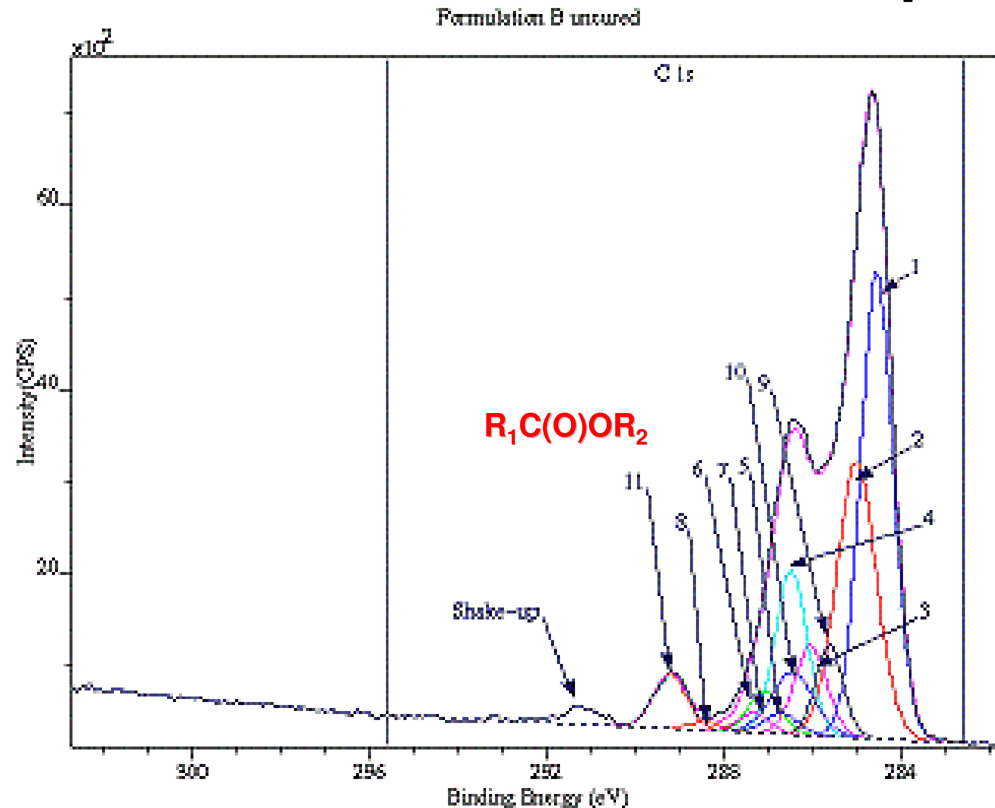

Espectro depois da cura com adição de poliéster. Picos 9, 10 e 11estão associados com poliéster mostrando que este aditivo é segregado para a superfície como esperado pelas sua baixa tensão superficial.

Estrutura Eletrônica de Polianilinas

PH. SNAUWAERT*, R. LAZZARONI*, J. RIGA and J. J. VERBIST**

Laboratoire de Spectroscopie Electronique, Facultés Universitaires Notre-Dame de la Paix, 61, rue de Bruxelles, B-5000 Namur (Belgium)

(Received March 10, 1986; in revised form July 1, 1986; accepted July 7, 1986)

246

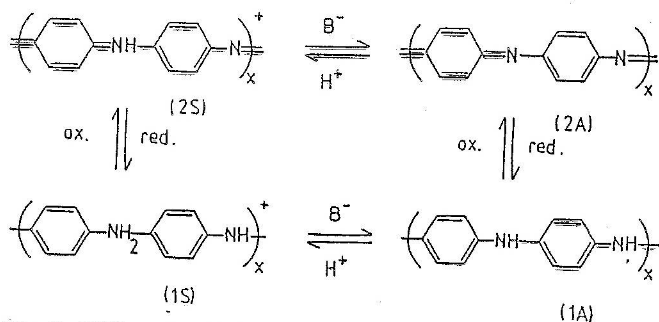

Fig. 1. Different acid–base and redox forms of polyaniline [12].

TABLE 1

XPS binding energies (eV) and doping levels (%) for polyaniline synthesized in thr
different media

Medium	E_b C 1s	E_b N 1s	E_b O 1s	Dopir level
Acid	285.9	400.8	533.4	19
Basic	286.0	400.7	533.1	5
Organic	285.8	400.8	533.4	12

Espectro da Banda de Valência via XPS

Polianilina

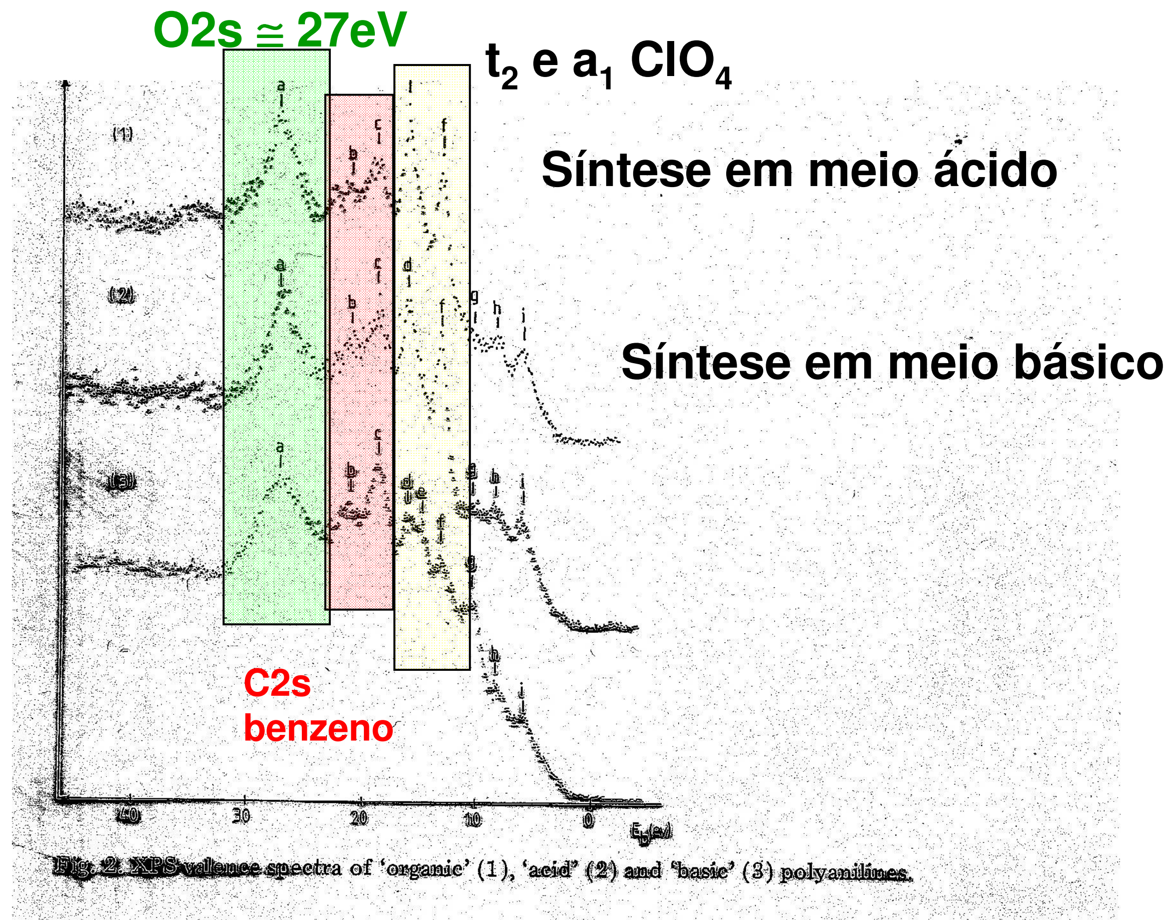

Cerâmicas

Trióxido de Selênio

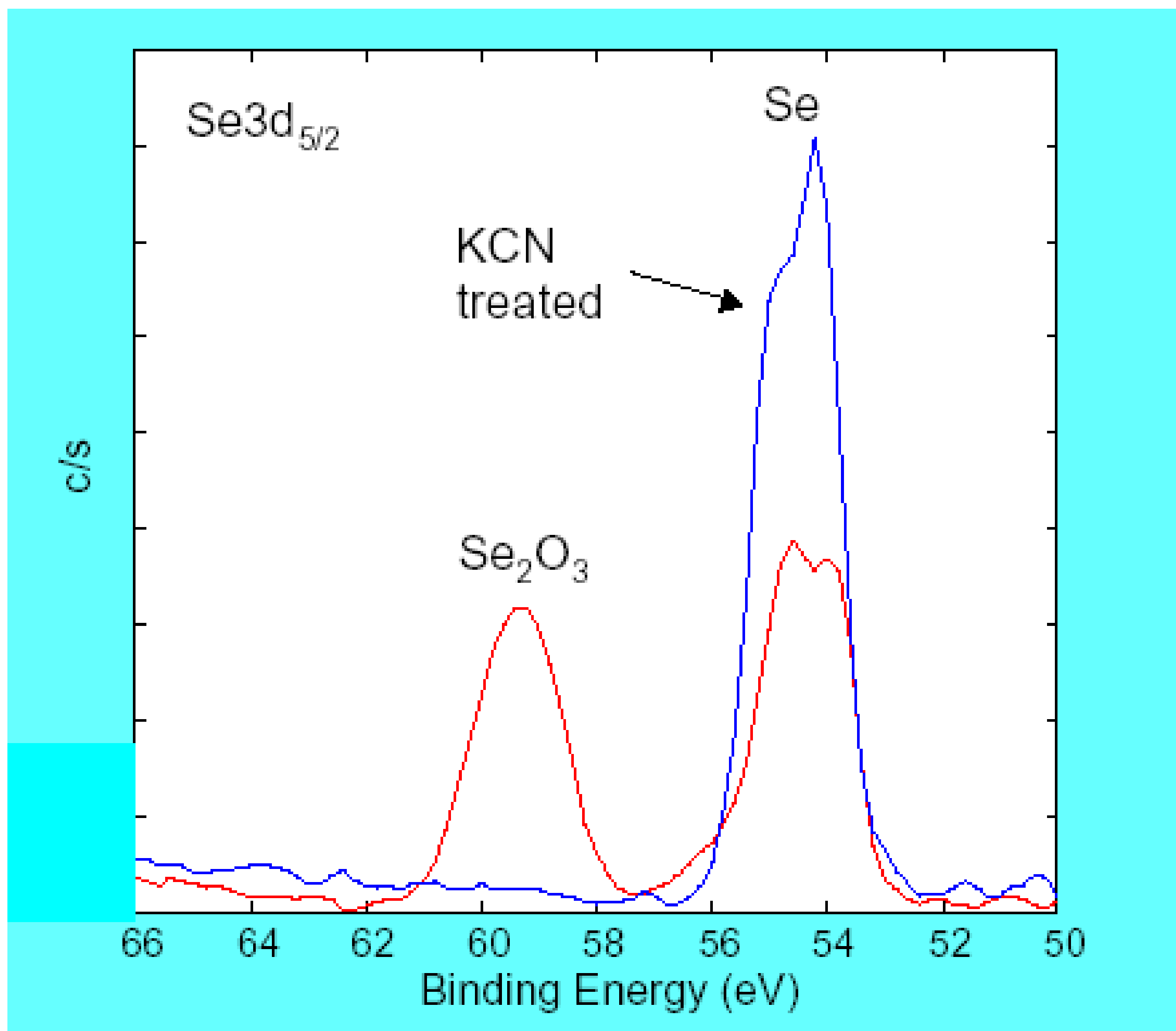

Dióxido de Titânio

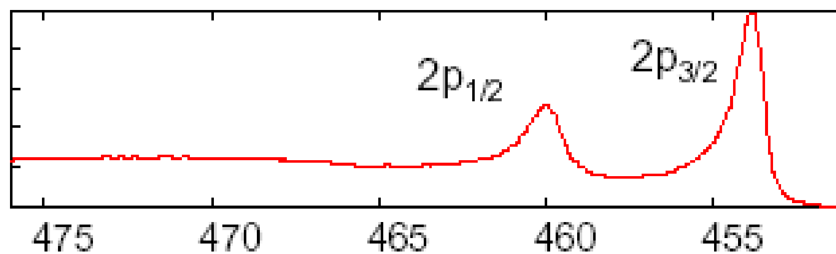

Ti metal peak (454 eV)

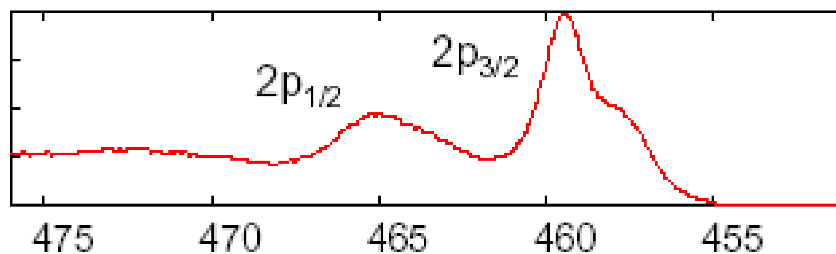

TiO_2 (110)
with some
reduced states

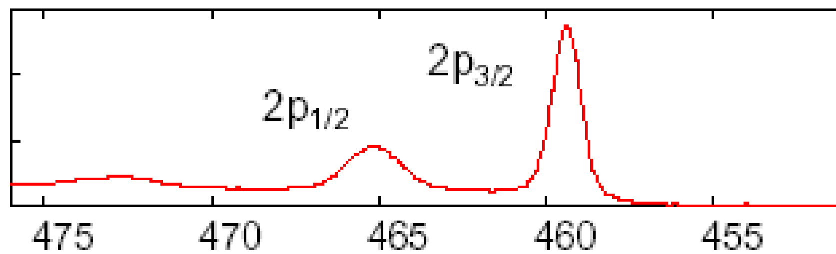

TiO_2 peak (459 eV)

Pico assimétrico = desconfie da presença de mais de uma espécie química

Identificação de Óxidos e Hidróxidos de Alumínio

Corundum Al_2O_3

Gibbsita γ-$Al(OH)_3$ monoclínico - a = 8.684 Å, b = 5.078 Å,c = 9.736 Å, β = 94.54°)

Bayerita β-$Al(OH)_3$ a = 5.0626 Å, b = 8.6719 Å, c = 9.4254 Å, β = 90.26°)

Bohemita γ-AlO(OH) ortorrômbico, a = 3.6936 Å, b =12.214 Å, c = 2.8679 Å

Pseudobohemita AlO(OH) ortorrômico

J. Theo Kloprogge[a,*], Loc V. Duong[a], Barry J. Wood[b], Ray L. Frost[a]

Journal of Colloid and Interface Science 296 (2006) 572–576

Hidróxidos de Alumínio

Linha de Fotoemissão O1s

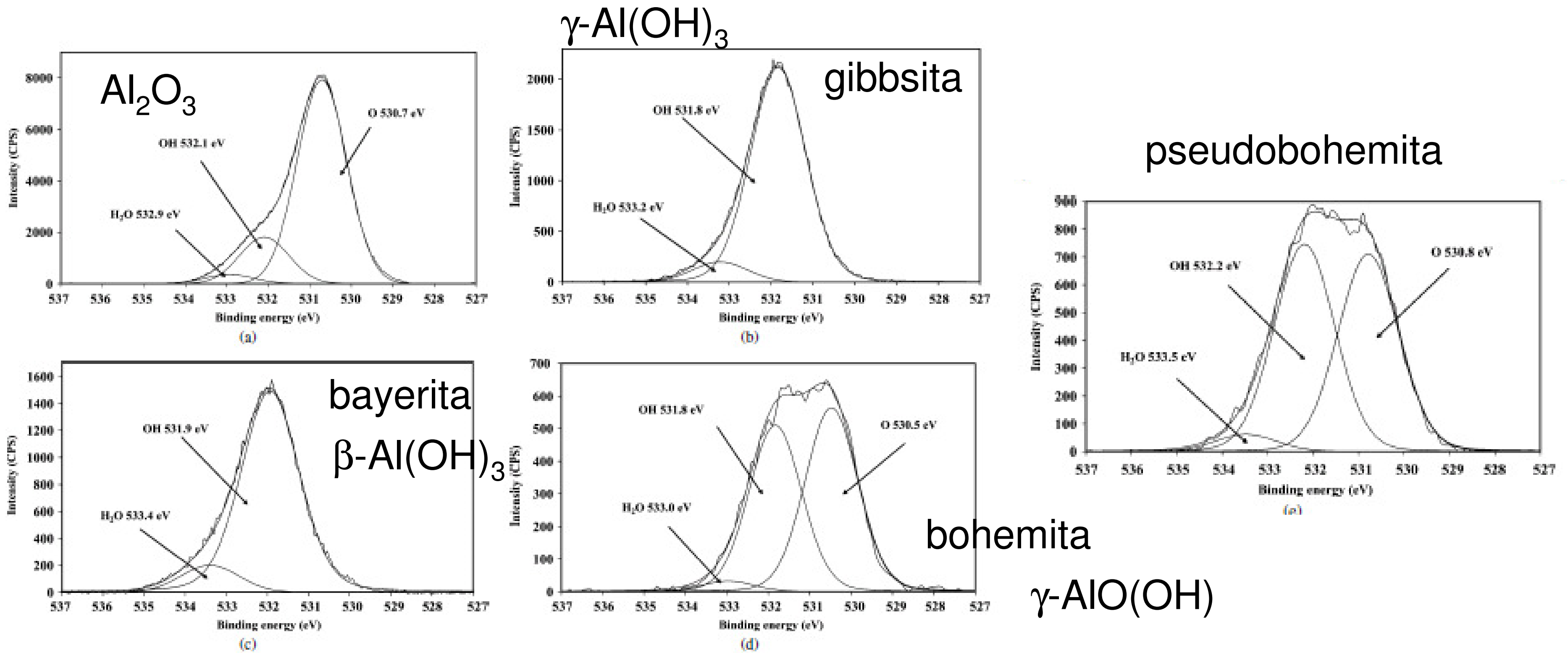

Hidróxidos de Alumínio
Linha de Fotoemissão Al2p

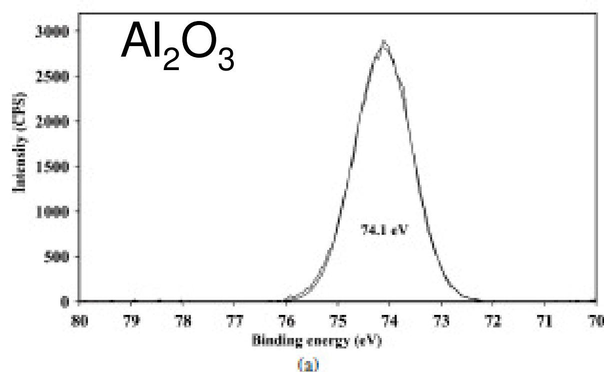

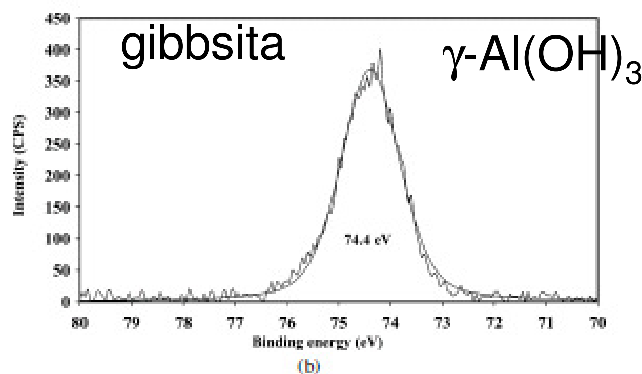

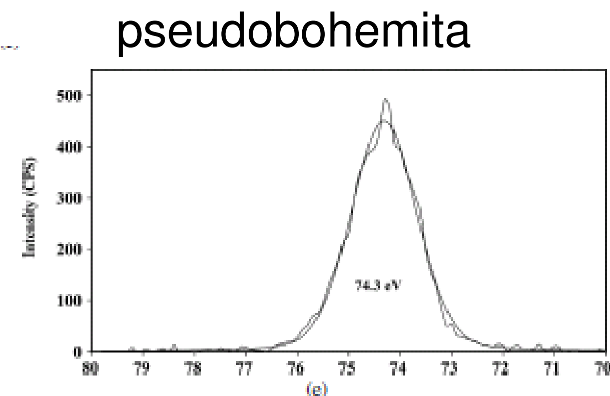

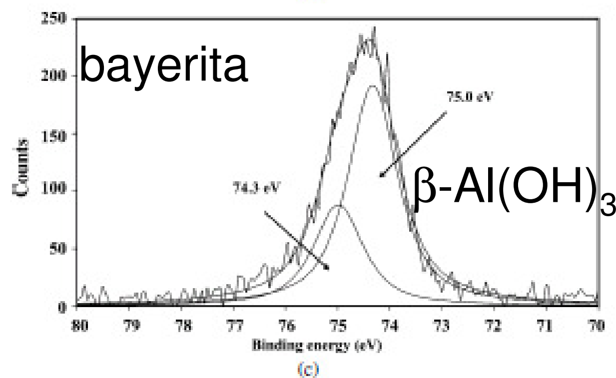

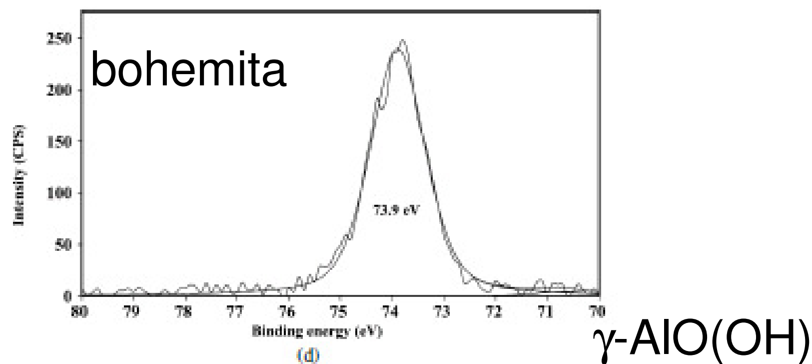

Hidróxidos de Alumínio

Composição Quimca da Superfície

Table 1

Chemical compositions (atom%) of the alumina phases based on the high resolution XPS analyses

	Corundum Al_2O_3	Gibbsite $Al(OH)_3$	Bayerite $Al(OH)_3$	Boehmite $Al(OOH)$	Pseudoboehmite $Al(OOH)$
O	61.62	72.89	68.78	67.55	62.54
Al	38.38	24.41	23.94	32.45	27.29
Na[a]	bd	2.69	4.83	bd[b]	bd
N[a]	bd	bd	1.78	bd	bd
Cl[a]	bd	bd	0.66	bd	1.35
Al/O molar ratio	0.63	0.33	0.34	0.48	0.43

[a] Impurities.
[b] bd—below detection limit.

Carbono Vítreo

Oxidação Eletroquímica

SHUJI YUMITORI
Kobe Steel, Ltd., Chemical Environmental Research Laboratory, Takatsukadai 1-5-5, Nishi-ku, Kobe 651-22, Japan

JOURNAL OF MATERIALS SCIENCE **35** (2000) 139–146

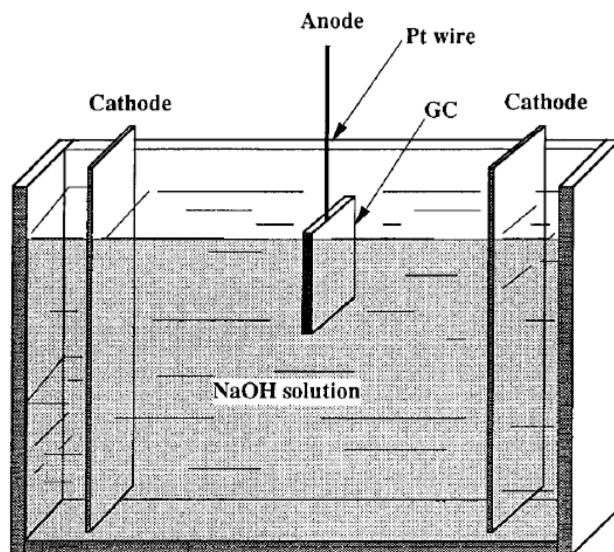

Figure 1 Apparatus for anodic oxidation.

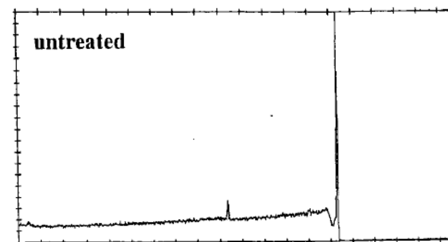

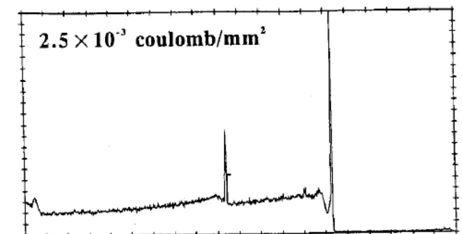

Carbono Vítreo

Oxidação Eletroquímica

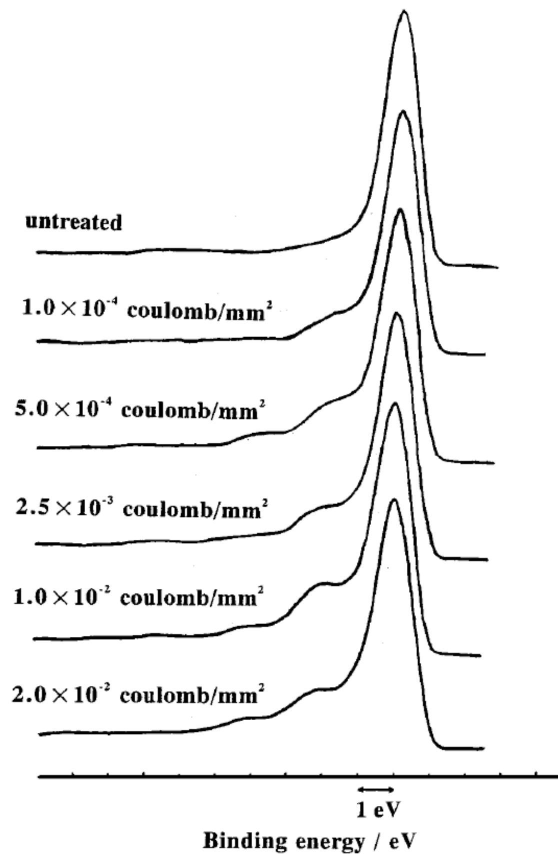

Figure 6 C_{1s} spectra of untreated and treated glass-like carbon at various electrical charges.

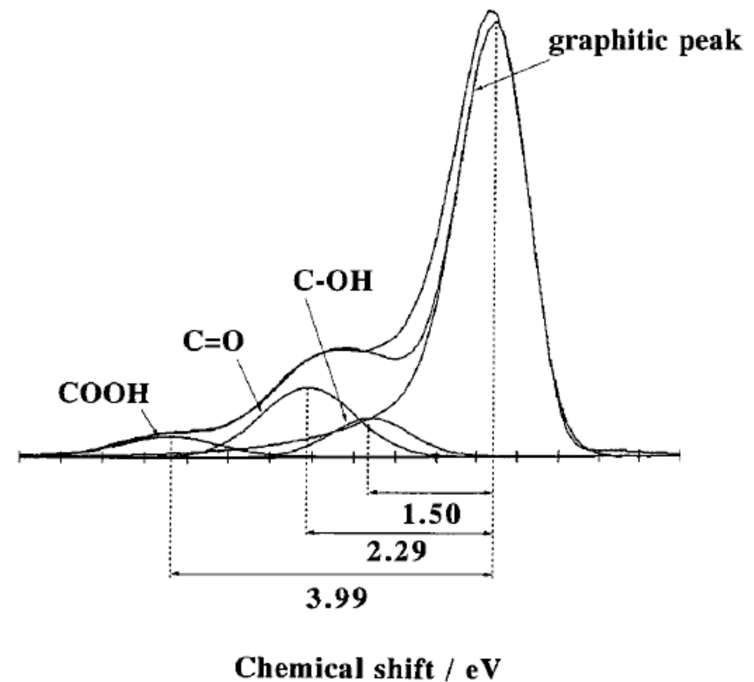

Figure 10 Asymmetric curve fitting of C_{1s} spectrum of glass-like carbon treated at 1.0×10^{-2} C/mm^2.

Carbono Vítreo

Oxidação Eletroquímica

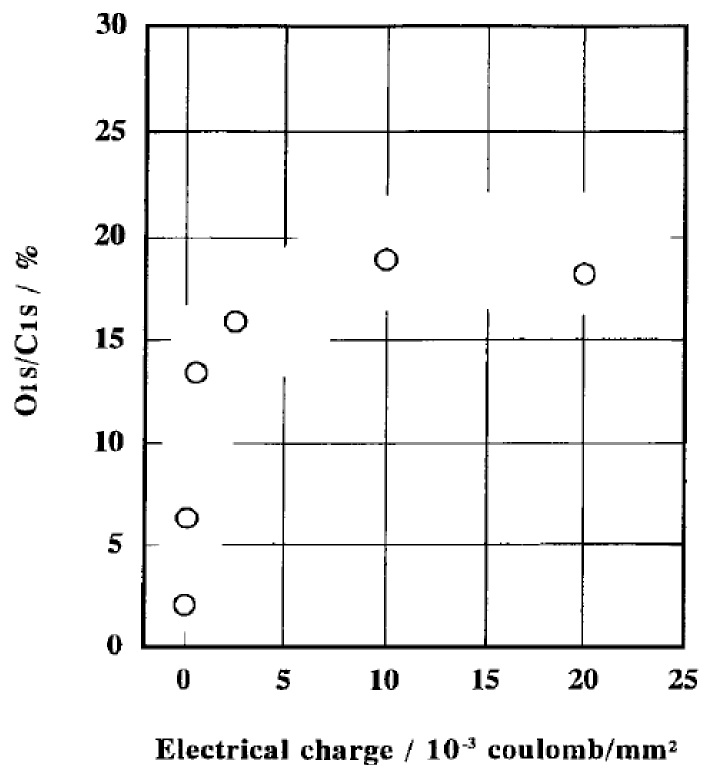

Figure 5 Effect of electrical charge on oxygen concentration of glass-like carbon.

TABLE III Peak area ratio of each functional group of each sample evaluated by the asymmetric curve fitting technique with 2nd graphitic peak

	Peak area ratio (%)		
Sample	C–OH	C=O	COOH
Untreated	—	—	—
Treated at 1.0×10^{-4} C/mm^2	6.99	—	—
Treated at 5.0×10^{-4} C/mm^2	11.95	—	3.61
Treated at 2.5×10^{-3} C/mm^2	—	11.06	2.56
Treated at 1.0×10^{-2} C/mm^2	—	16.14	3.49
Treated at 2.0×10^{-2} C/mm^2	—	12.14	4.19

Vidro de Silicato Alcalino

Superfície

D. Sprenger [a,1], H. Bach [b], W. Meisel [a] and P. Gütlich [a]

Journal of Non-Crystalline Solids 159 (1993) 187–203

Table 1
Properties of the glass samples

Melt number	Melt composition	Melt educts (mol%)
A–687	$11.11Na_2O \cdot 88.88SiO_2$	10.00% Na_2CO_3 88.60% SiO_2 1.6% $NaNO_3$
B–10026	$15Na_2O \cdot 85SiO_2$	15.40% Na_2CO_3 84.60% SiO_2 0.3% As_2O_3
B–10027	$25Na_2O \cdot 75SiO_2$	25.59% Na_2CO_3 74.41% SiO_2 0.3% As_2O_3
A–688	$25Na_2O \cdot 75SiO_2$	24.00% Na_2CO_3 74.40% SiO_2 1.6% $NaNO_3$
B–10028	$30Na_2O \cdot 70SiO_2$	30.66% Na_2CO_3 69.34% SiO_2 0.3% As_2O_3
B–10029	$35Na_2O \cdot 65SiO_2$	35.71% Na_2CO_3 64.29% SiO_2 0.3% As_2O_3
B–10030	$40Na_2O \cdot 60SiO_2$	40.75% Na_2CO_3 59.25% SiO_2 0.3% As_2O_3
B–10031	$45Na_2O \cdot 55SiO_2$	45.77% Na_2CO_3 54.23% SiO_2 0.3% As_2O_3

- Cada cátion de metal alcalino cria um par de elétrons não ligantes pela quebra de uma ligação Si-O-Si (siloxano).

Non-bonded oxygen = NBO (oxigênio terminal)

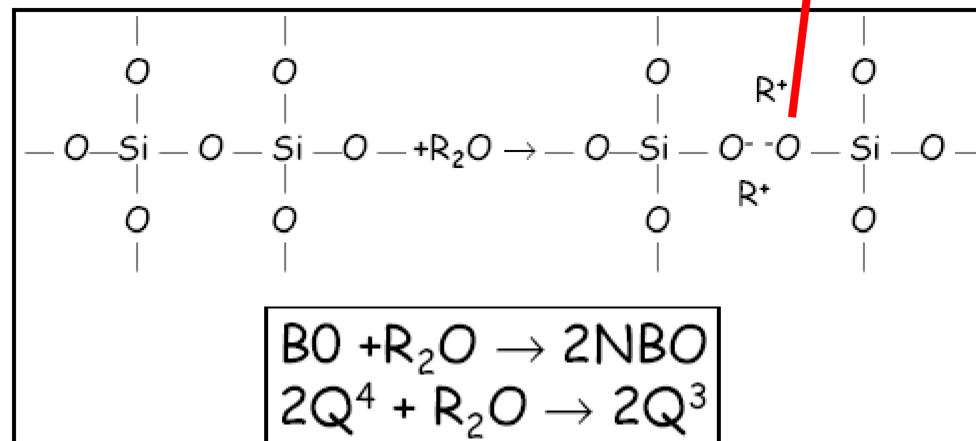

XPS O1s

Quartzo vs Silicato Alcalino

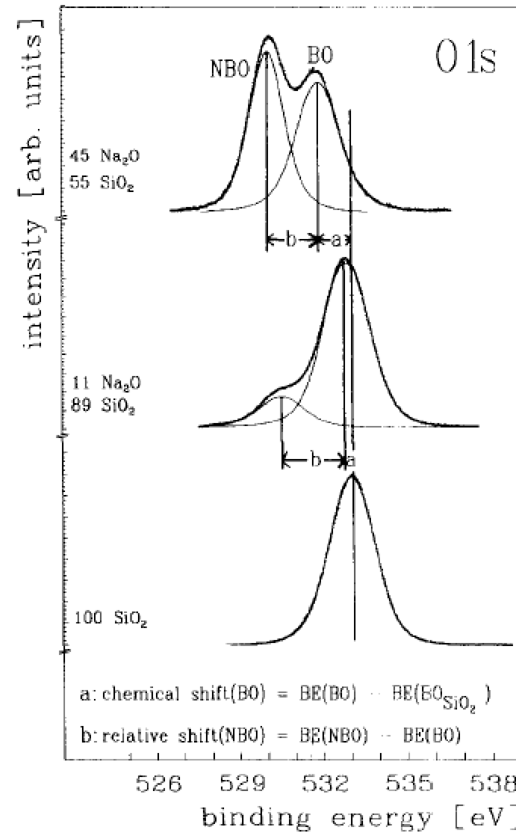

Fig. 2. O 1s spectra of a quartz glass, an $11Na_2O \cdot 89SiO_2$ glass, and a $45Na_2O \cdot 55SiO_2$ glass. The distance *a* represents the chemical shift of the BO in the sodium silicate glass relative to the BO in fused silica (vitreous silica); the distance *b* (relative shift) is the energy difference between the NBO and the BO.

Silicatos Alacalinos

Modelo Estrutural

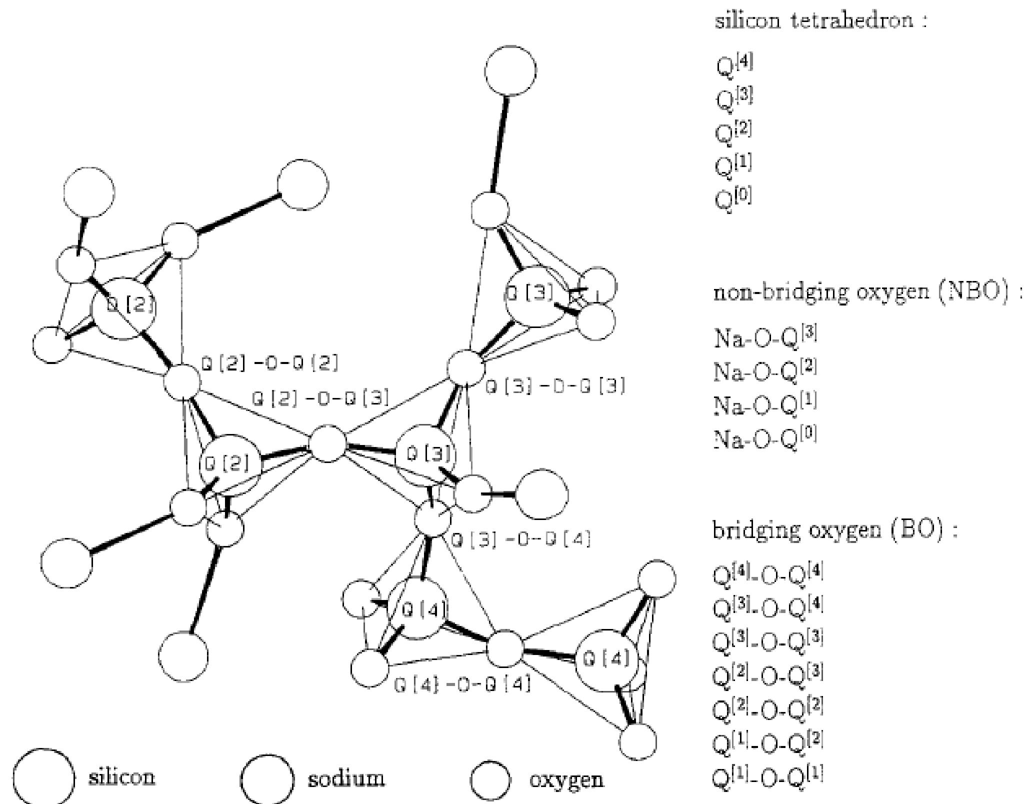

Fig. 6. Model of a sodium silicate network presenting the different oxygen bonds in sodium silicate glasses up to a concentration of 50% Na_2O. This figure does not consider the limitations of the binary model and the discrete bond model, because an oxygen bond distribution like this is to be expected in a molten glass only.

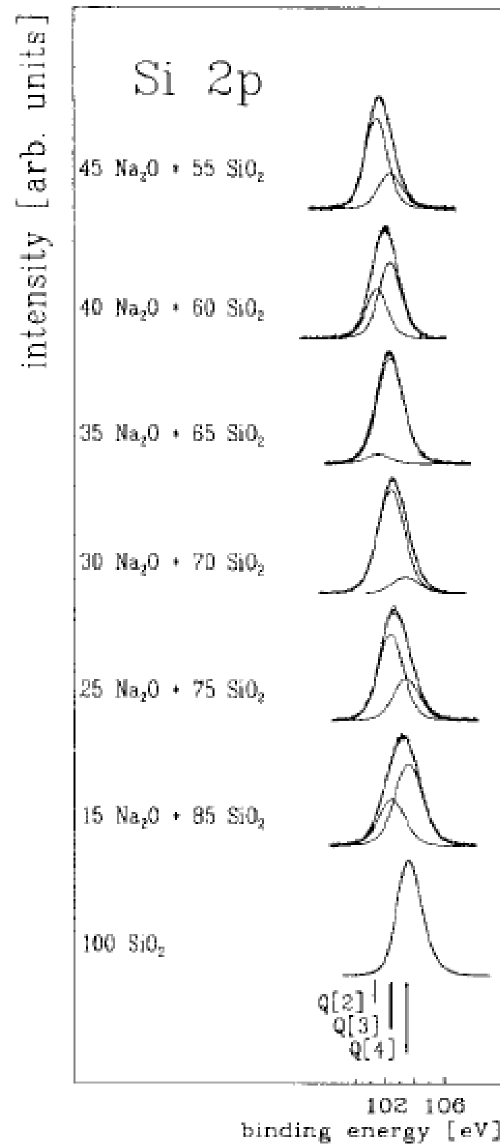

Fig. 9. Subspectra representing different $Q^{[i]}$ species, fitted to Si 2p spectra of sodium silicate glasses of different compositions and of a Herasil glass, after background subtraction.

XP-O1s

Silicato Alcalino

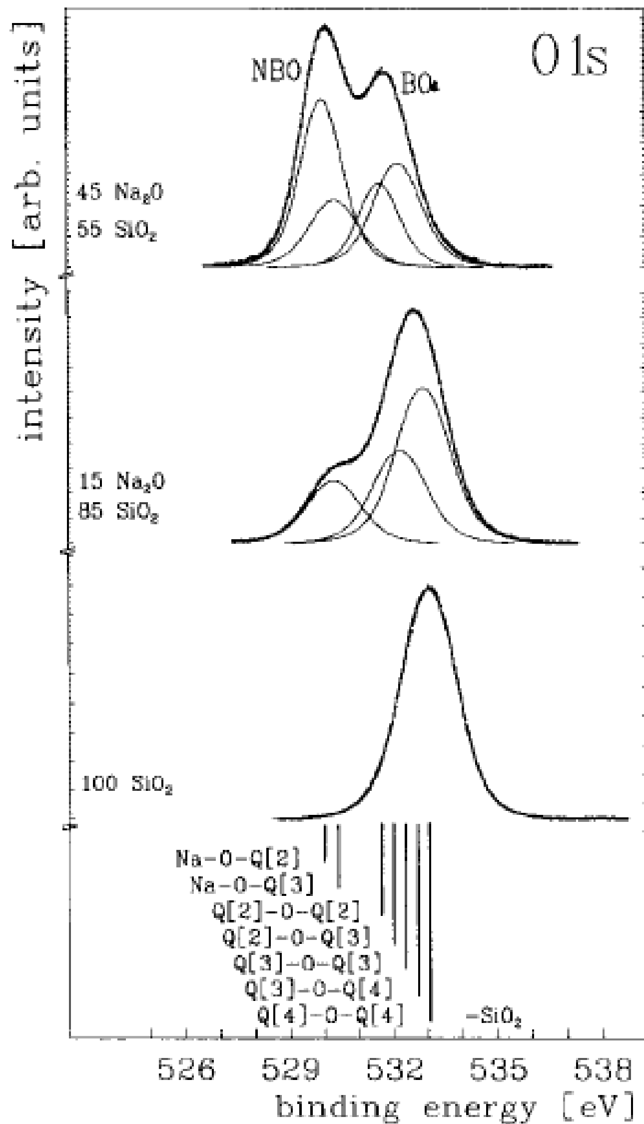

Fig. 11. Interpretation of the relative and absolute chemical shifts (see fig. 2) of the measured O 1s signal by a superposition of the different oxygen bonds as calculated by the DBM for the BO as well as for the NBO. (It should be mentioned that, because of a small amount of metasilicate in the $45Na_2O \cdot 55SiO_2$ glass block (see table 1), the composition of the glass sample is close to 44 mol% Na_2O and, therefore, the subline intensity ratio differs slightly from that in fig. 10.)

Silicatos
Banda de Valência

Diagrama de Orbitais Moleculares Moleculas Modelo de Silicatos

Tetralquilortosilicatos

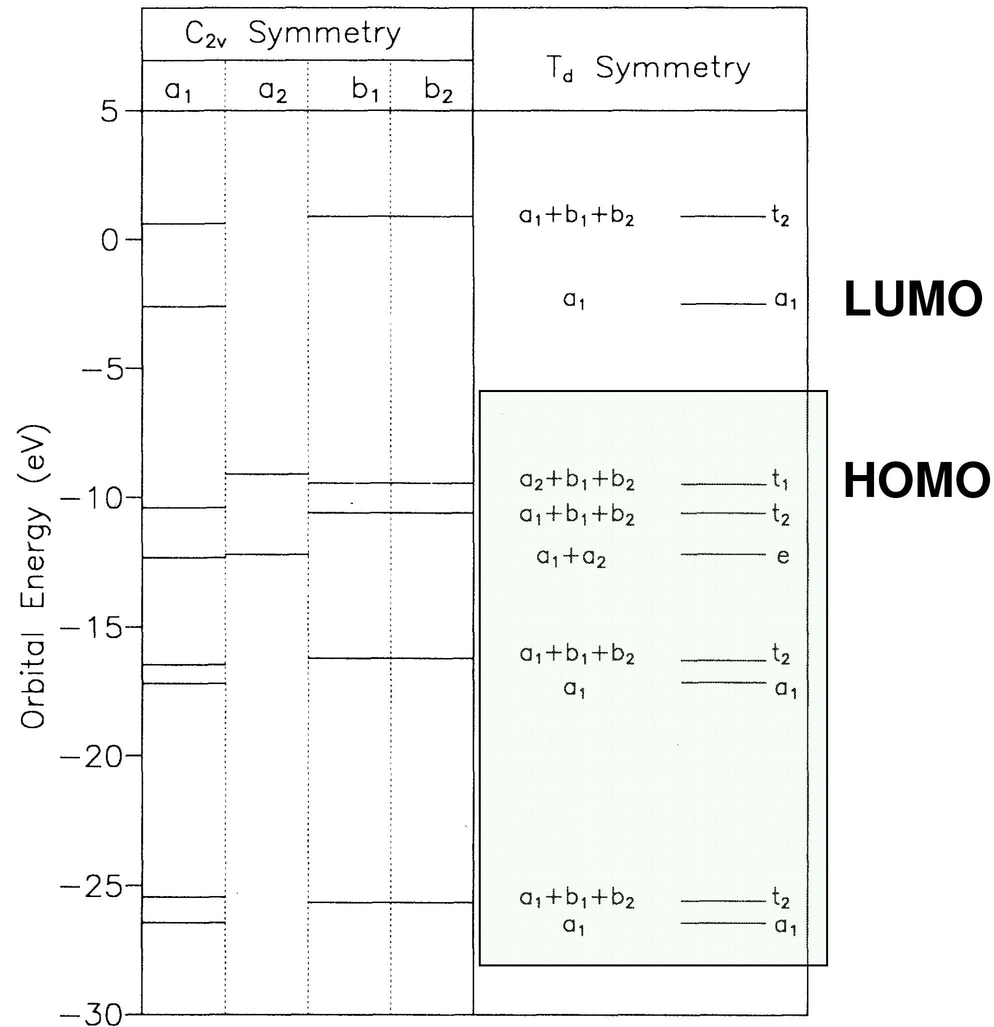

D. G. J. Sutherland, M. Kasrai, G. M. Bancroft,* Z. F. Liu, and K. H. Tan **Phys.Rev.B, 48(23), 14989, 1983.**

XP-VB

Counts

1000
800
600
400
200
0

a1
C–H
t2
C–O
e
t2
t1

18.0 16.0 14.0 12.0 10.0 8.0

Binding Energy (eV)

α-Quartzo

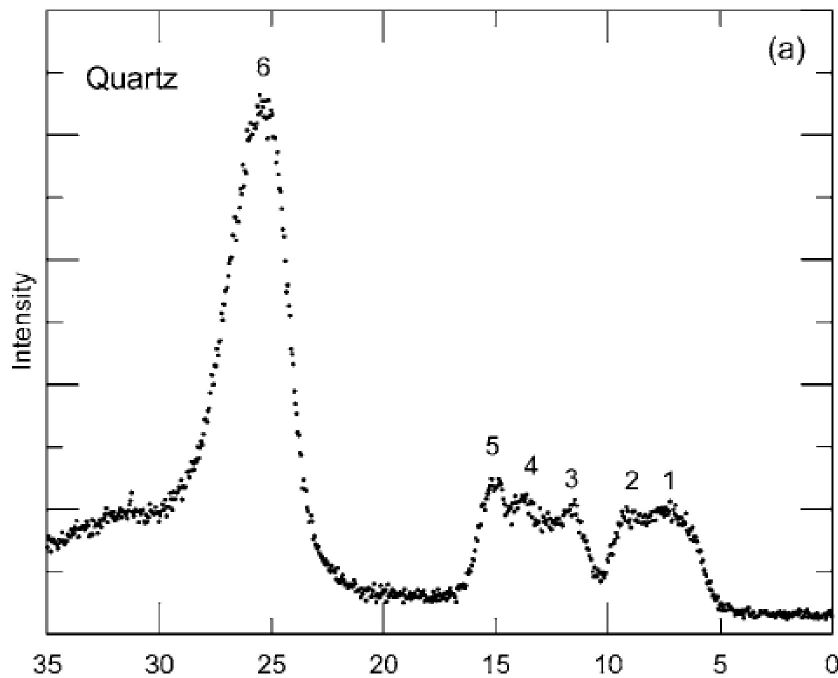

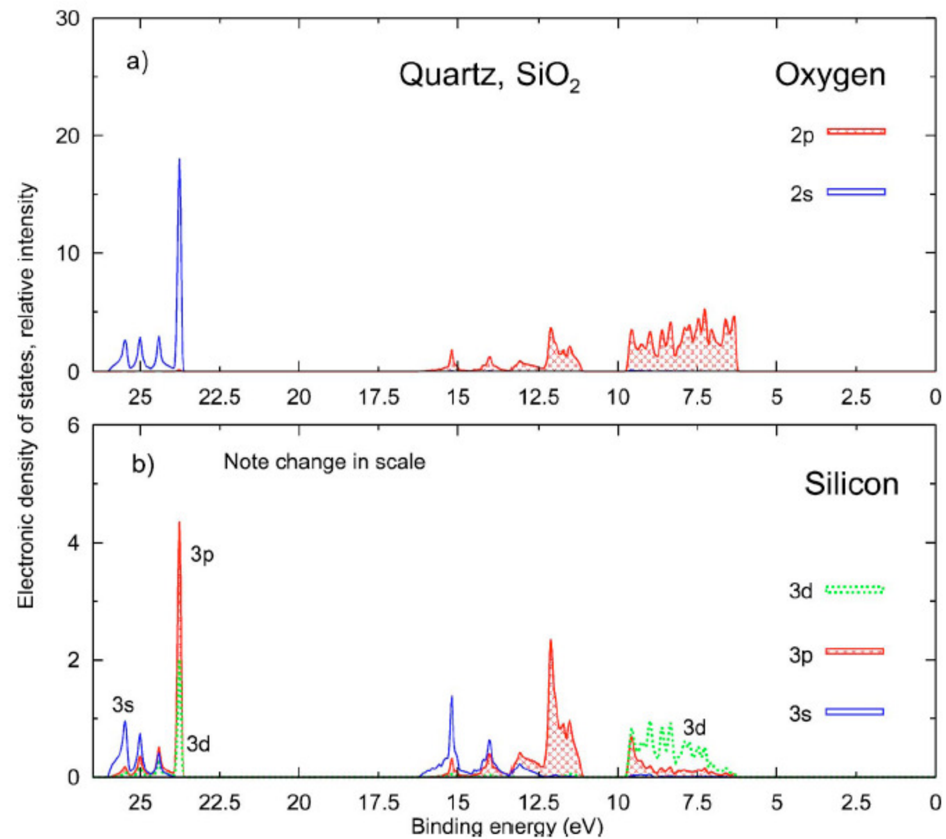

Perceba a similariedade entre o espectro do quartzo e do $Si(OEt)_4$

Crystal Orbital Overlap Population (COOP) Analysis para o DOS do Quartzo

XP-O2s e BV
Silicatos Alcalinos

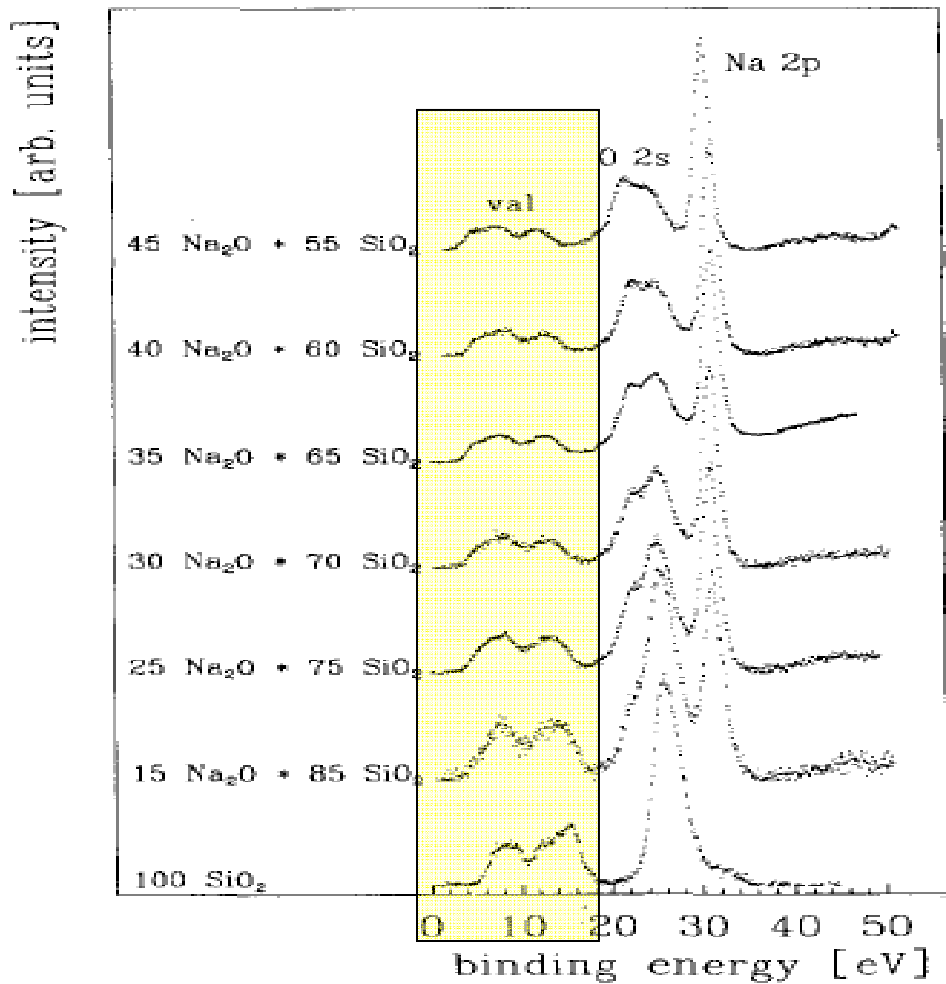

BV :

Materiais Compósitos

Estudo de Estrutura de Madeiras

O navio de guerra do século XVII da marinha sueca, cujo nome era *Vasa*, está no Vasa Museum desde 1990. Neste ano, ele foi resgato da baía de Estocolmo onde afundou em 1628. Após uma restauração a estrutura de madeira parecia em boa forma quando começou a se detectar um espalhamento de enxofre e sulfato pela estrutura. A fim de estudar o processo corrosivo em andamento foi feito um estudo por XANES e XPS.

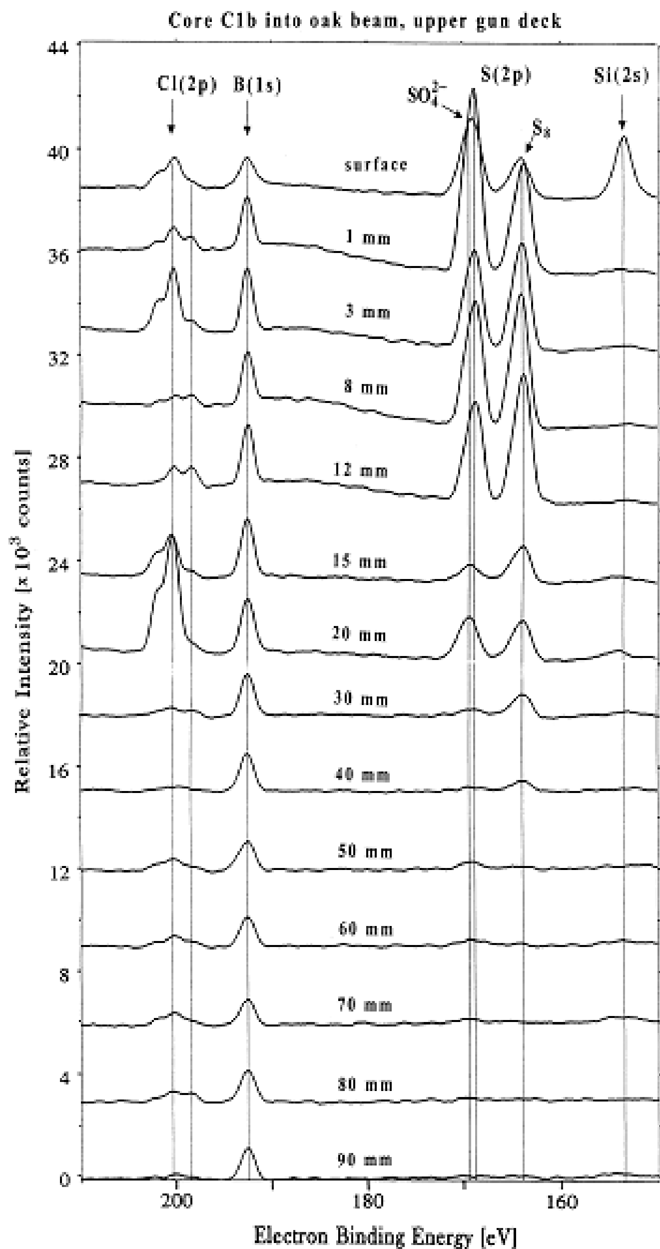

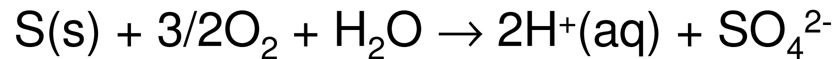

$$S(s) + 3/2O_2 + H_2O \rightarrow 2H^+(aq) + SO_4^{2-}$$

A reação acima demonstra a formação de sulfato a partir de enxofre no casco do navio. Esta reação é catalisado por íons Fe^{3+} originário da corrosão da peças em metal do navio. O enxofre elementar é proveniente do ácido sulfídrico formado pelas bactérias anaeróbicas do fundo do mar. O H_2S penetra a madeira e se deposita na forma de enxofre elementar. Ao retiramos o navio do fundo do mar expomos o enxofre a uma atmosfera aeróbica que propicia a lenta formação de sulfato.

Sandström, M., Jalilehvand, F., Persson, I., Gelius, U., Frank, P., Hall-Roth, I., Deterioration of the 17th-century warship Vasa by internal formation of sulphuric acid, *Nature* **415**, 893-897 (2002) .

XPS e Adsorção

Adsorção

Deslocamento nos Picos de Fotoemissão da Banda de Valência de Semicondutores

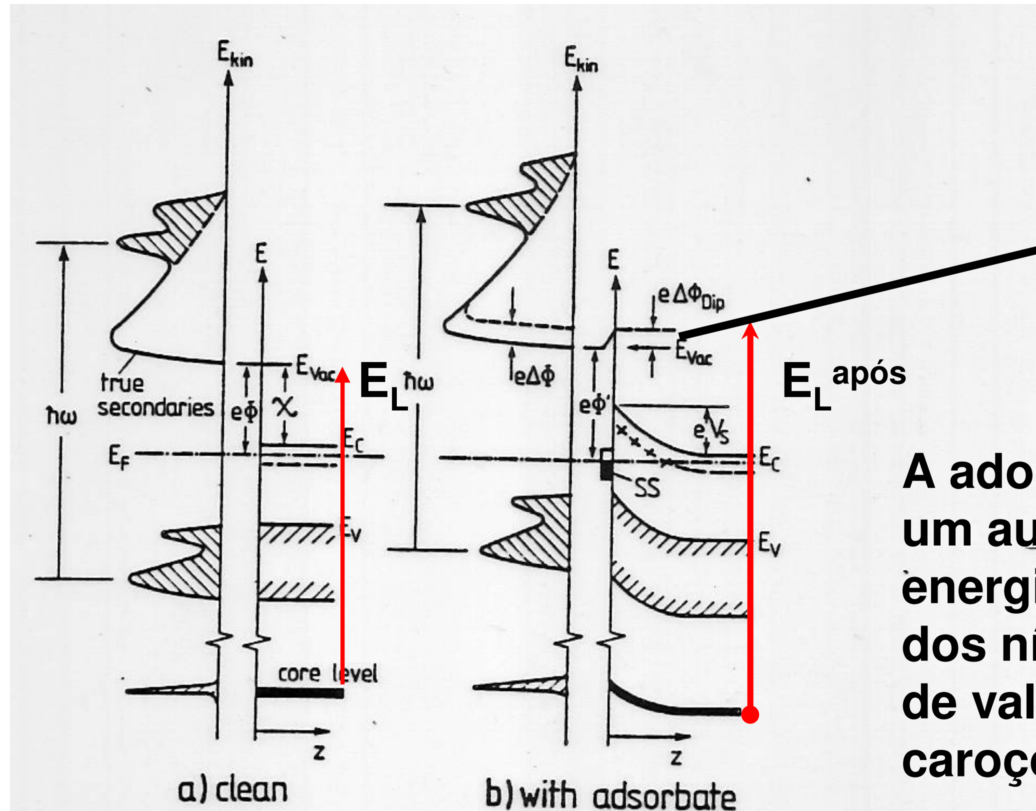

Fig. XV.2a,b. Explanation of adsorbate-induced changes in the photoemission spectrum of a semiconductor: (**a**) Photoemission process on the clean surface of a semiconductor. Photons of energy $\hbar\omega$ excite electrons from the valence band (upper edge E_V) into empty states, from where they leave the crystal and are detected with a kinetic energy above the vacuum energy E_{vac}. True secondary electrons arise from multiple scattering events within the crystal. (**b**) An adsorbate induces extrinsic Surface States (SS) in the bulk band gap and an upwards band bending eV_S. This changes the work function from $e\phi$ to $e\phi'$. Simultaneously with the shift in valence and conduction band states, core level states also shift upwards in energy at the surface

Aumento ($e\Delta\o_{DIP}$) da função trabalho devido à adsorção.

A adosrção provoca um aumento da energia de ligação dos níveis da banda de valência e de caroço do

Xe adsorvido sobre Pd(001)

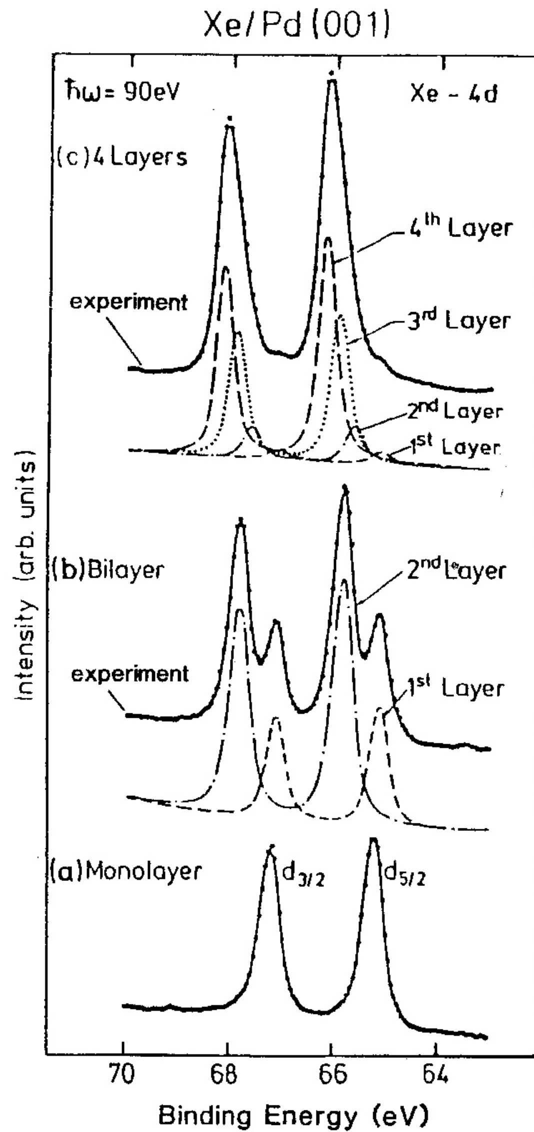

Fig.2.34. Xe 4d core-level PE spectra for (a) a monolayer, (b) a bilayer and (c) four layers of Xe on Pd(001). The binding energies are with respect to the vacuum level of the adsorbate covered substrate. The solid curves are the result of a least-squares fit of the experimental data (full dots) to (a) one spectrum, (b) two spectra (1st and 2nd layer) and (c) 4 spectra (1st to 4th layer) [2.76]

Pt sobre SiO_2/Si

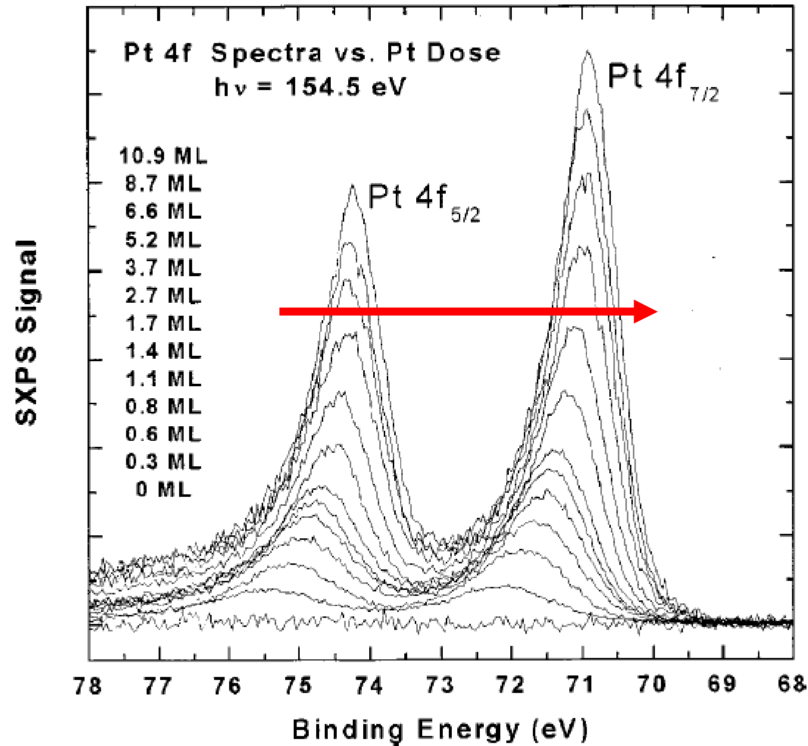

FIG. 1. SXPS Pt $4f$ data for dosing on flat, amorphous SiO_2, measured at a photon energy of 154.5 eV. The peak height increases monotonically with dose for coverages of up to ~11 ML.

$$\mathrm{BE}=\mathrm{BE}_0+\Delta\mathrm{BE},$$

$$\Delta\mathrm{BE}=\mathrm{q}\cdot V=e\cdot\left(\frac{1}{4\pi\epsilon_0}\cdot\frac{e}{R}\right),$$

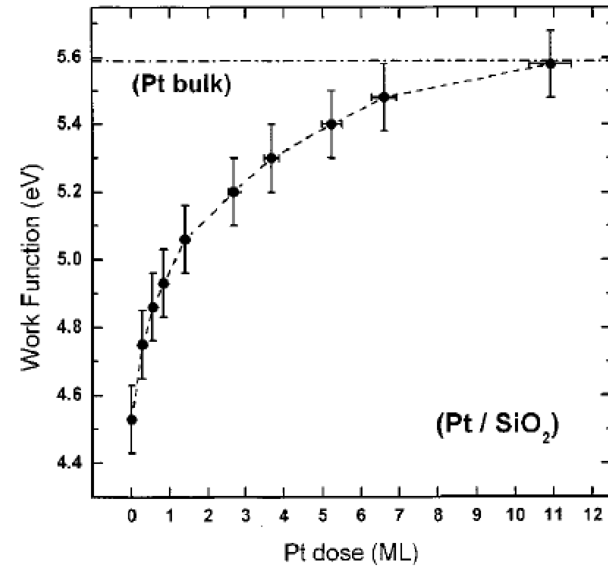

FIG. 3. Work function of the Pt-dosed SiO_2 film as a function of Pt dose, which rises monotonically until the bulk Pt value of 5.59 eV (Ref. 9) is asymptotically reached. A dashed line is drawn between consecutive points as a guide to the eye.

J. Vac. Sci. Technol. B 18(4), Jul/Aug 2000

Pt sobre SiO_2/Si

Função Doniac-Sunjic

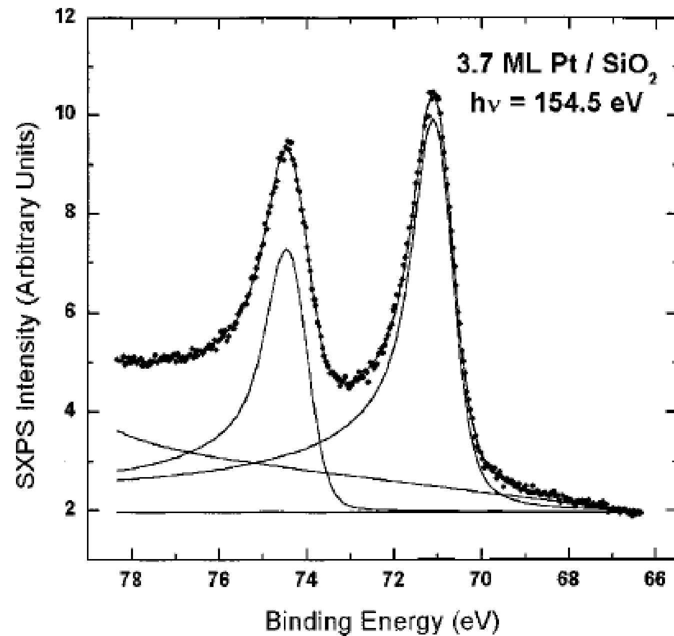

FIG. 4. Example fit of Gaussian-broadened Doniach–Sujic line shape to the Pt 4*f* peaks at an intermediate dose of 3.7 ML. Individual contributions to the fit are shown below the data.

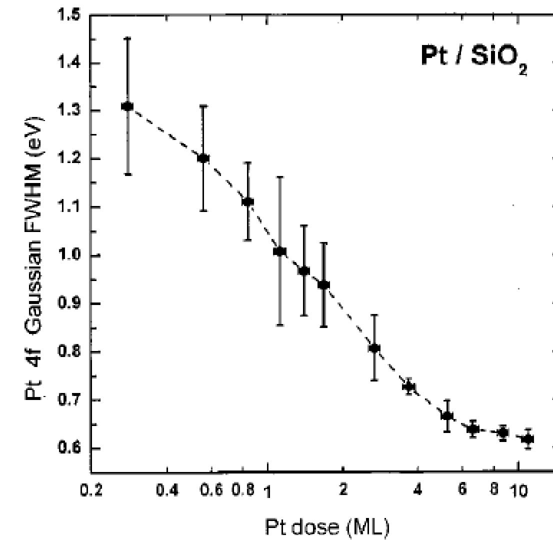

FIG. 5. Gaussian full width at half maximum (FWHM) of the Pt 4*f* peaks measured as a function of Pt dose. The monotonic decrease is taken to indicate that the clusters approach uniform bulk Pt by smoothly coalescing as more Pt is available, until the intrinsic bulk linewidth is approached, to within experimental resolution. A dashed line is drawn between consecutive points as a guide to the eye.

Deslocamento Químico

Dimensionalidade dos Clusters Metálicos

$$\Delta \mathrm{BE} \propto \theta^{-1/D},$$

Expoente -1/2 indica crescimento 2D
Expoente -1/3 indica crescimento 3D

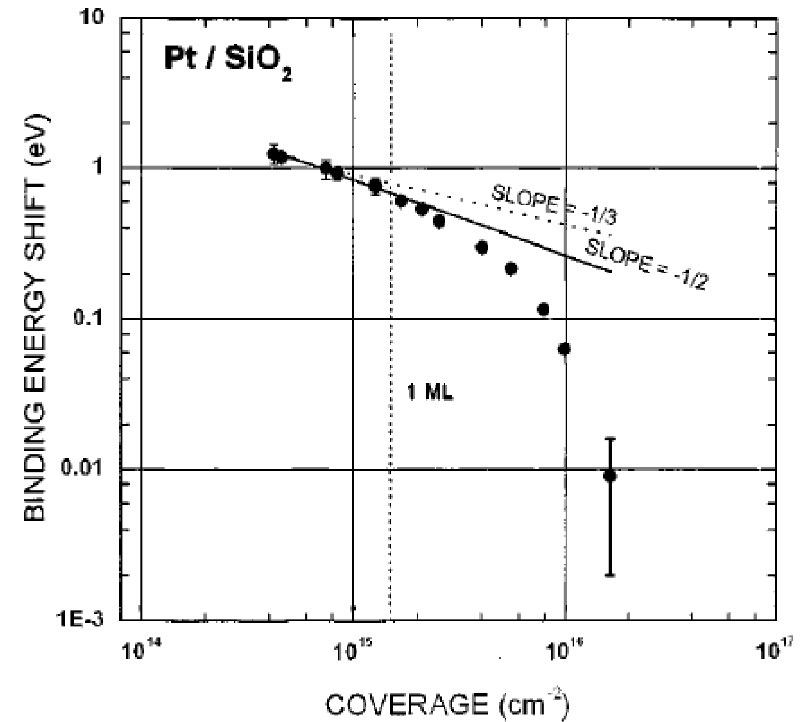

FIG. 7. Log–log plot of binding energy shift vs Pt dose reveals the growth order as the slope. Here, two-dimensional growth is implied by the slope of −1/2.

Filmes Automontados de Tióis sobre Au(111)

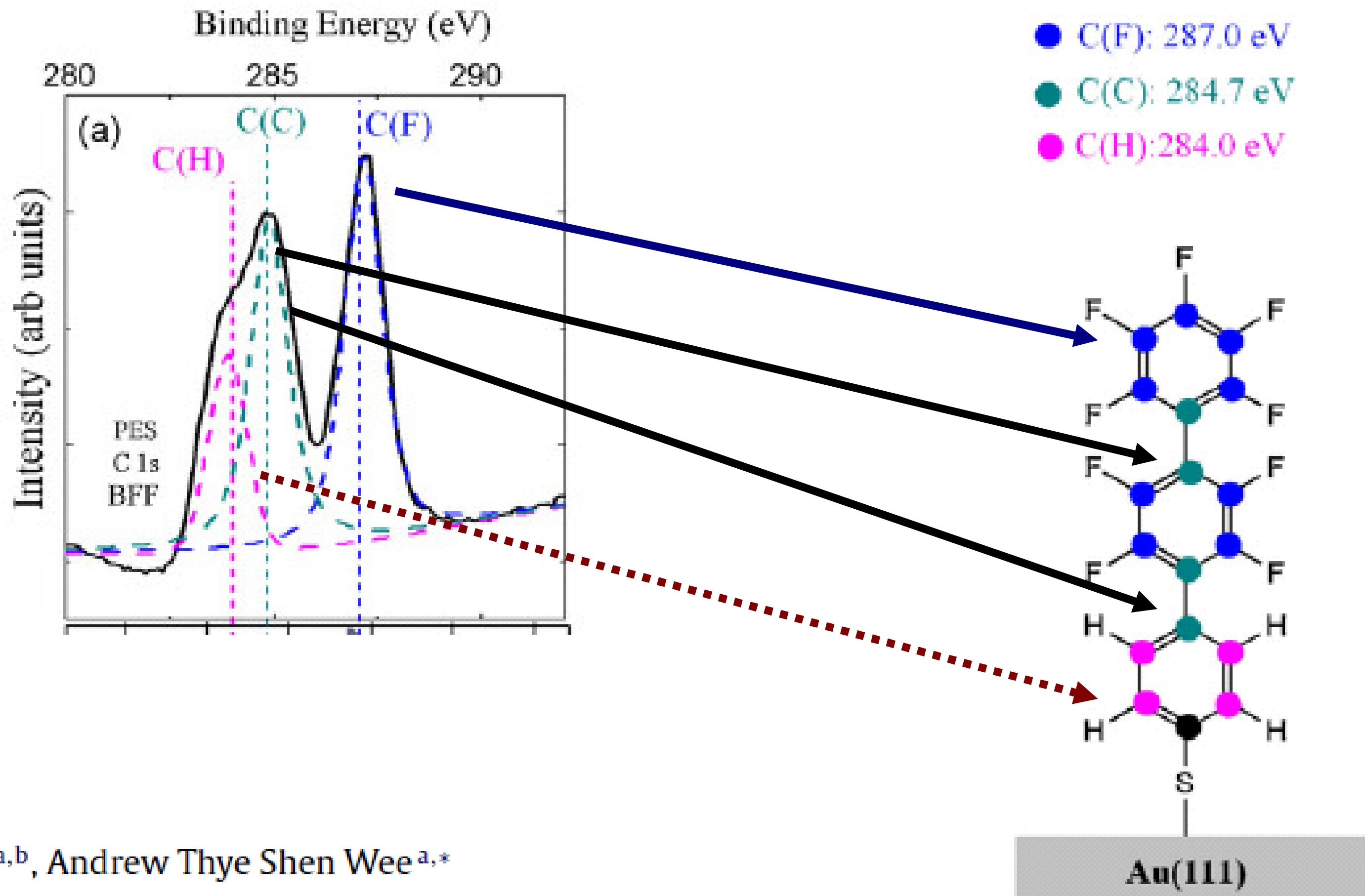

Wei Chen[a,b], Andrew Thye Shen Wee[a,*]

Journal of Electron Spectroscopy and Related Phenomena 172 (2009) 54–63

Self-assembled monolayers of semifluorinated thiols on electrochemically modified polycrystalline nickel surfaces

L. Tortech [a,b], Z. Mekhalif [b], J. Delhalle [b], F. Guittard [a], S. Géribaldi [a,*]

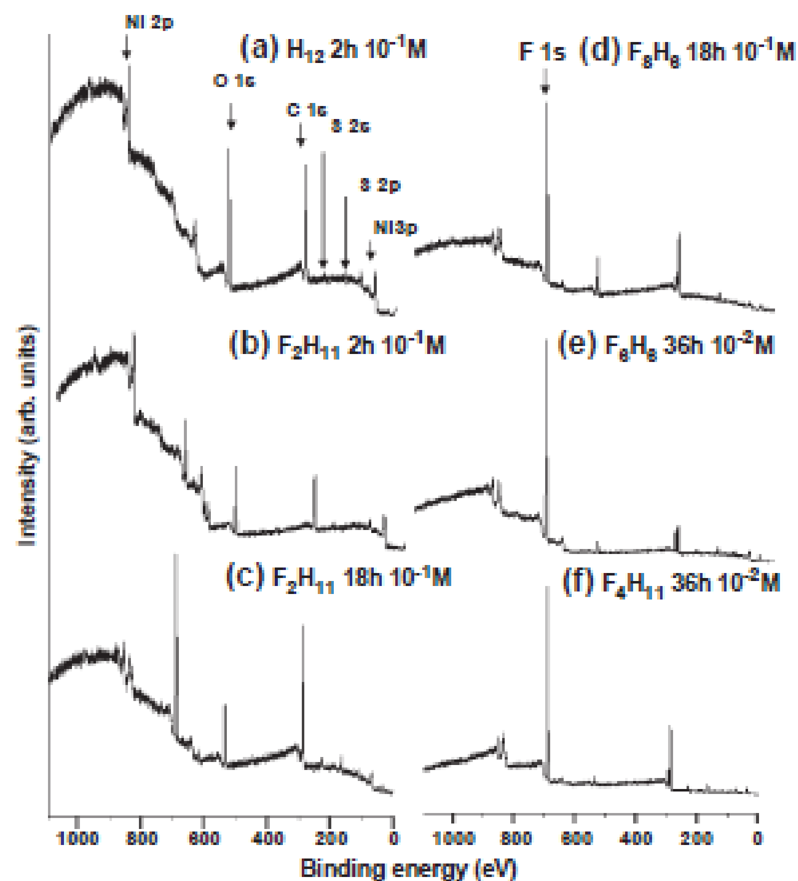

Fig. 1. Selection of XPS survey spectra of the Ni_{red} substrates modified with *n*-dodecanethiol (H_{12}) and semi-fluorinated alkanethiols (F_mH_n).

Thin Solid Films 491 (2005) 253 – 259

Linha de Fotoemissão C1s

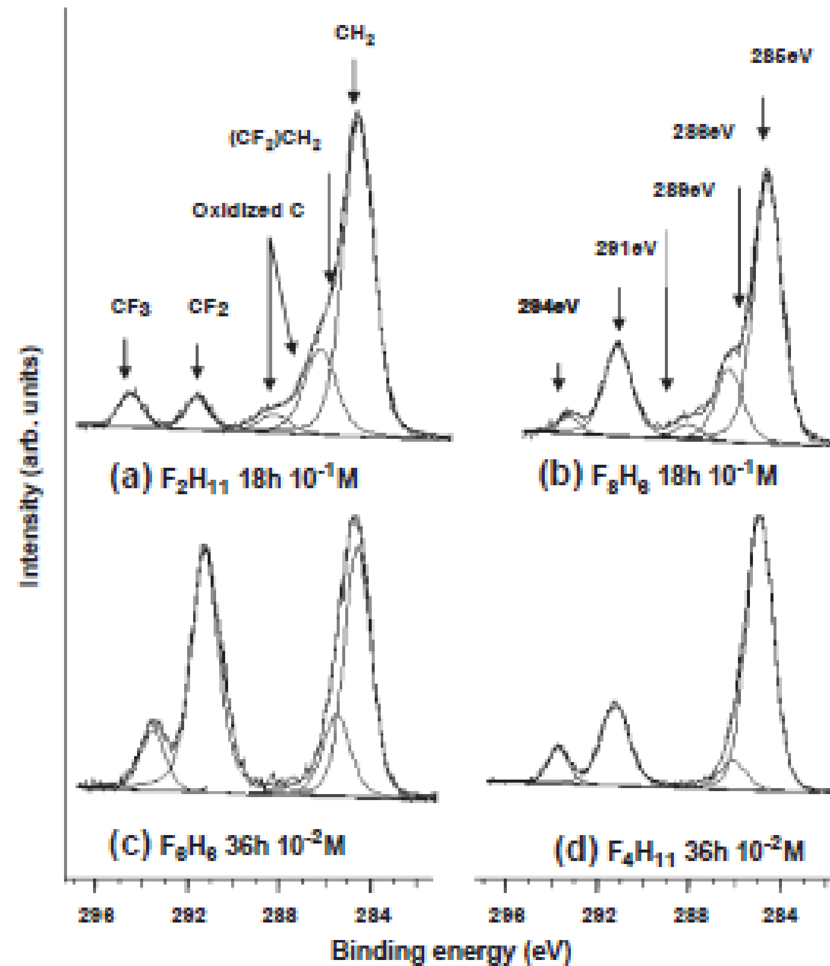

Fig. 2. XPS C 1s level of Ni_{sol} substrates modified with F_mH_n monolayer at different concentrations and dipping times.

Linha de Fotoemissão S2p

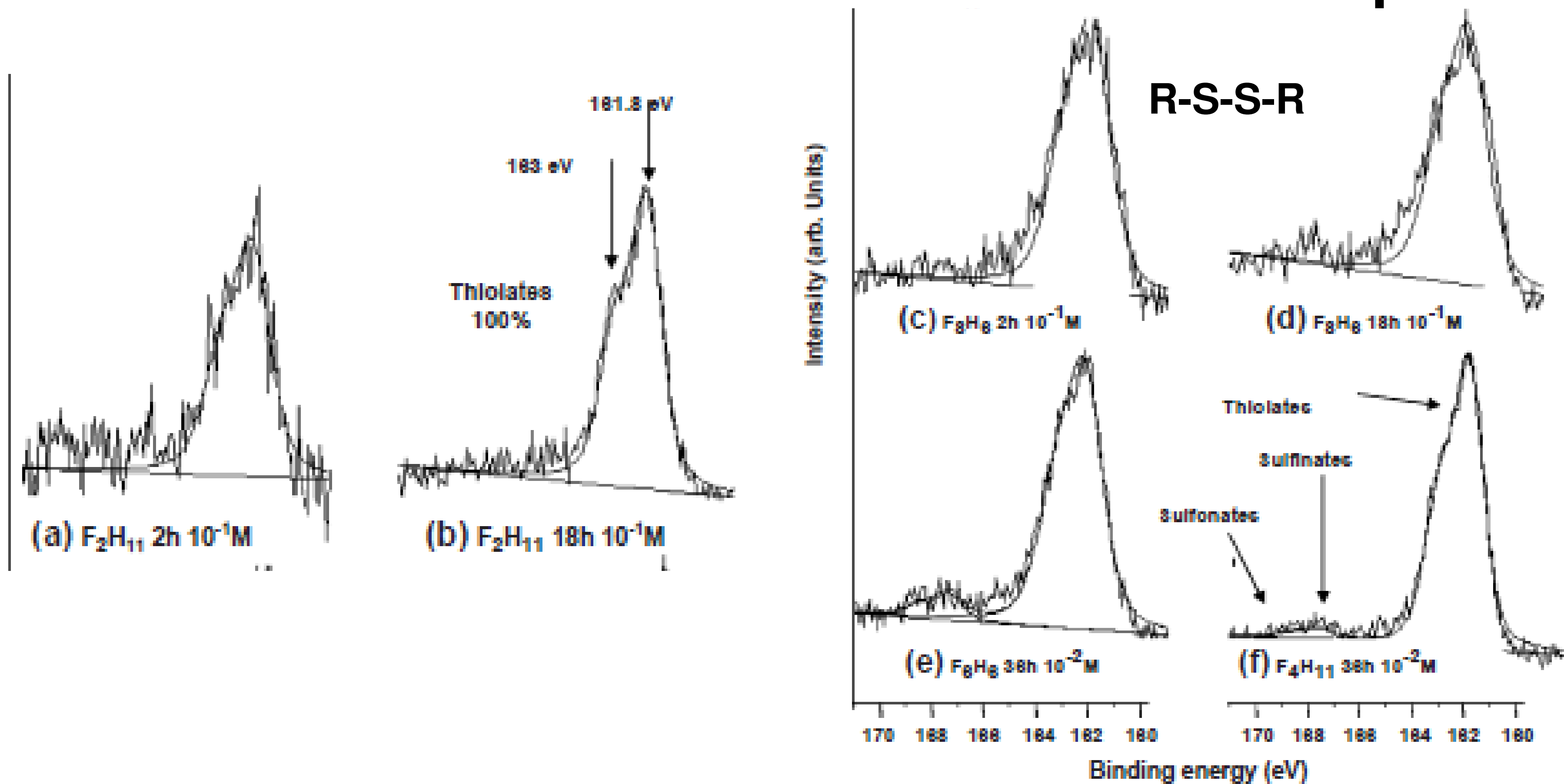

Fig. 4. XPS spectra of the S 2p core level for the fluorinated monolayers at various concentrations and various dipping times.

X-ray Studies of Self-Assembled Organic Monolayers Grown on Hydrogen-Terminated Si(111)

Hua Jin,† C. Reagan Kinser,† Paul A. Bertin,‡ Donald E. Kramer,† Joseph A. Libera,† Mark C. Hersam,† Sonbinh T. Nguyen,‡ and Michael J. Bedzyk*,†

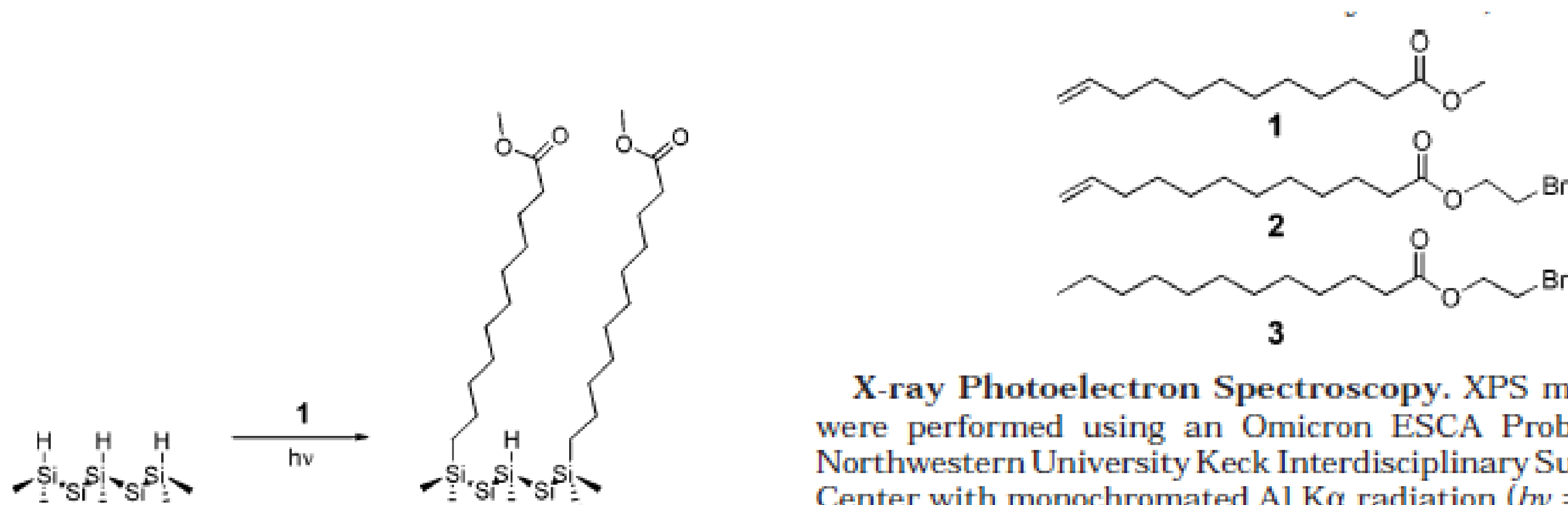

Figure 1. Schematic representation of the process to prepare SAM-**1**.

X-ray Photoelectron Spectroscopy. XPS measurements were performed using an Omicron ESCA Probe located at Northwestern University Keck Interdisciplinary Surface Science Center with monochromated Al Kα radiation ($h\nu = 1486.6$ eV). The sample was oriented with a 45° photoelectron takeoff angle from the sample surface to the hemispherical analyzer. An analyzer pass energy of 50 eV with 500 meV steps was used for single-sweep survey scans. High-resolution spectra were averaged over three sweeps using an analyzer pass energy of 17 eV with 20 meV steps. Unless otherwise noted, samples were ultrasonicated in CH_2Cl_2 and methanol for 2 min prior to XPS analysis. XPS spectra analyses were performed using XPSPeak 4.1.[22] Peaks were fit with a Gaussian−Lorentzian sum function after a Shirley background subtraction.

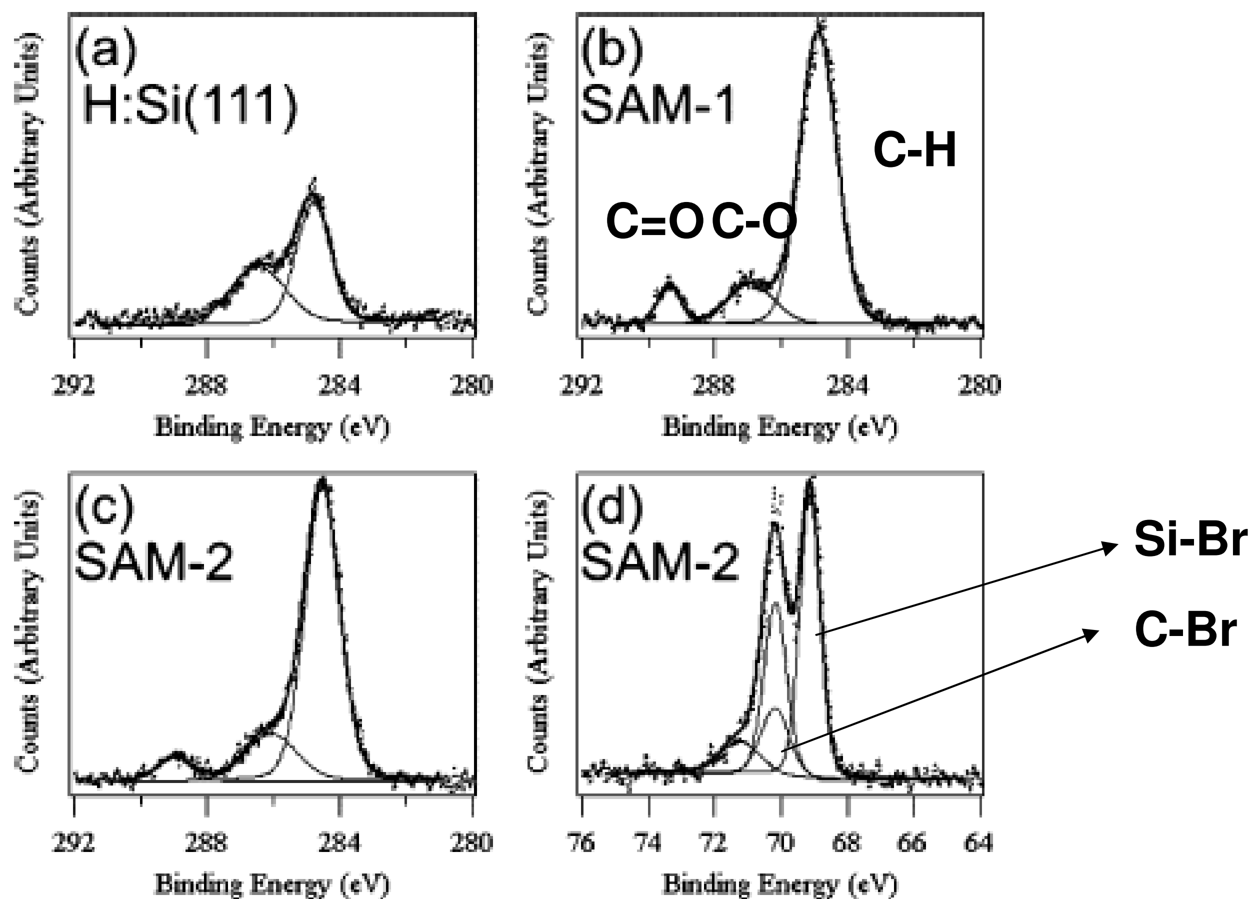

Figure 3. High-resolution XP spectra of H−Si(111) (a), SAM-**1** (b), and SAM-**2** (c,d). The C_{1s} region is shown in parts a−c, and the Br_{3d} region in part d. The carbon spectra show peaks at 284.5, 286.0, and 288.8 eV assigned to the aliphatic, carboxy, and carbonyl carbons, respectively. The carbonyl peak is characteristic of the ester functionality in compounds **1** and **2**. The bromine spectrum shows a convolution of two pairs of spin-doublets at 70.1 and 71.2 eV and at 69.1 and 70.2 eV assigned to carbon- and silicon-bound bromine, respectively.

Filmes Metalorgânicos sobre SiO_2/ Si(100)

Layer Design:

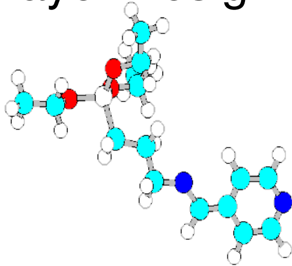

3-(imidazolylpropyl)propyltriethoxysilane
(3-IPTS)

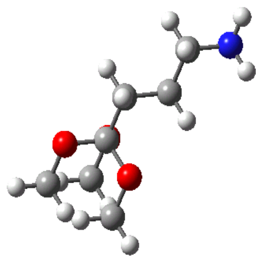

3-(aminolpropyl) ltrimethoxysilane **(3-APTS)**

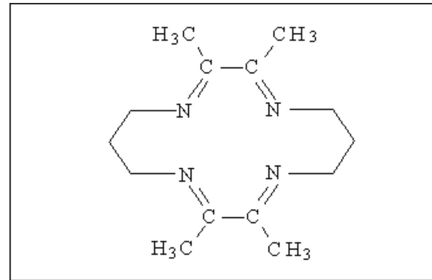

TIM

: hydrogen

: carbon

: nitrogen

: iron or silicon

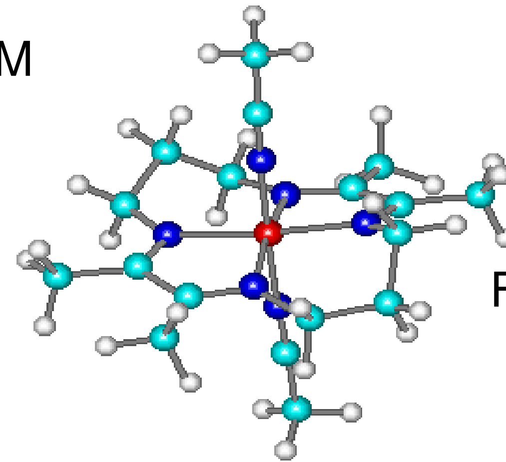

FeTIM

✓bis(N-acetonitrile)(N,N,N,N-2,3,9,10-tetramethyl-1,4,8,11-tetraazacyclotetradeca-1,3,8,10-tetraene)iron(II)

✓$[FeTIM(CH_3CN)_2]^{2+}$

Sililação do SiO_2/Si(100)

- Andresa, J.S. et al, Journal of Colloid and Interface Science 286 (2005) 303–309

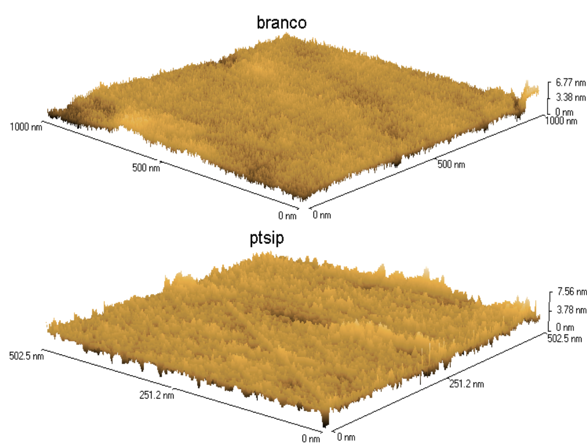

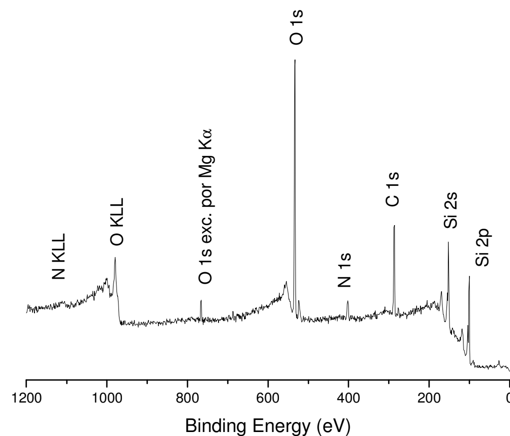

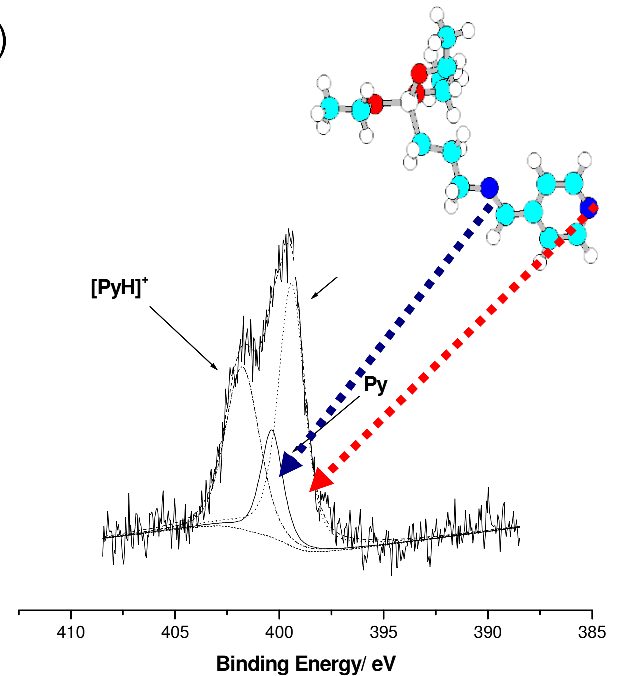

AFM image, Tapping mode, of the (A) SiO_2/Si and (B) 4PTSIP/SiO_2/Si (adsorption time of 150min).

XP-xpectra of 4-PTSIP a) Long-scan e b) high resolution N1s region.

FeTIM Adsorption on Silane Layer

Andresa et all, Surface and Interface Analysis

Samples	*E. L. (±0.3eV) Fe 2p*		*Ref*
FeTIM(acn)/Au	**710.3**	**714.3**	**1**
FeTIM(Him)/Au	**708.3**	**713.0**	**This work**
FeTIM/3-ImPTS[a]	**706.9**	**711.3**	**This work**
FeTIM/3-ImPTS[b]	**707.3**	**711.2**	**This work**

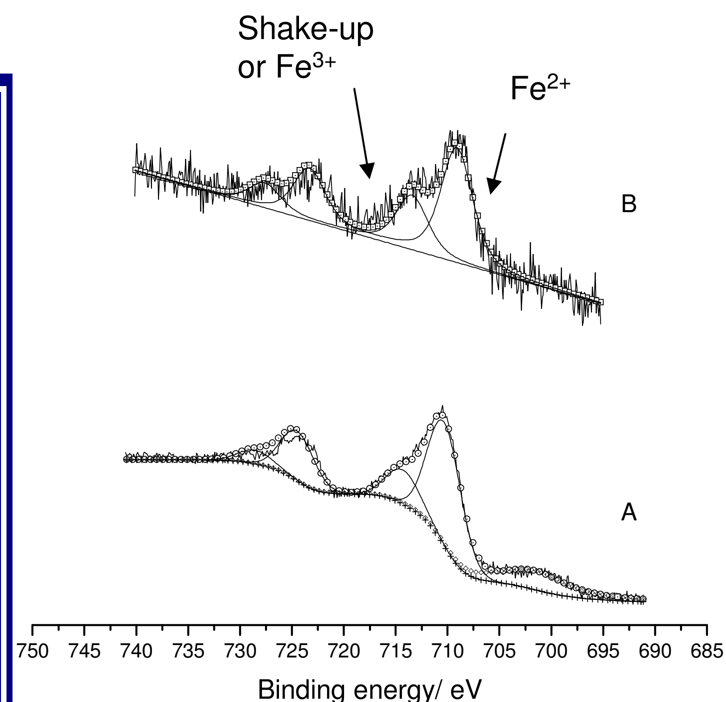

XP-spectra, Fe 2p region, of the (A) thin film of [FeTIM(CH3CN)2] (PF6)2 on gold and (B) adsorbed on 3-APTS/SiO2/Si.

Adsorção de Polioxoânions do tipo Keggin sobre SiO_2/Si(100) sililado

Keggin Heteropolyaninons

X = B, Si, Ge, P^{v} , As^{v}

M = Mo ou W

Polyanions with molecular formula $[XM_{12}O_{40}]^{n-}$.

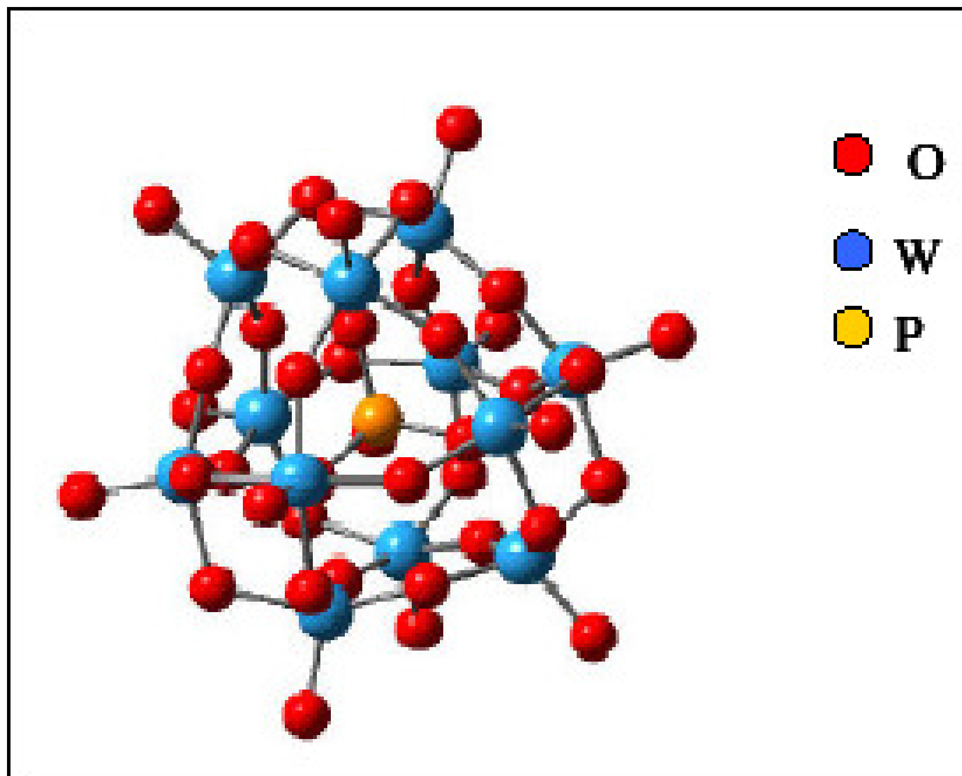

Phosphotungstic Acid

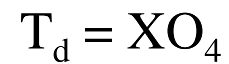

.

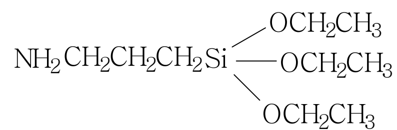

APTS

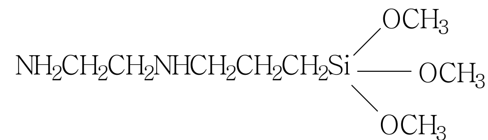

TSPEN

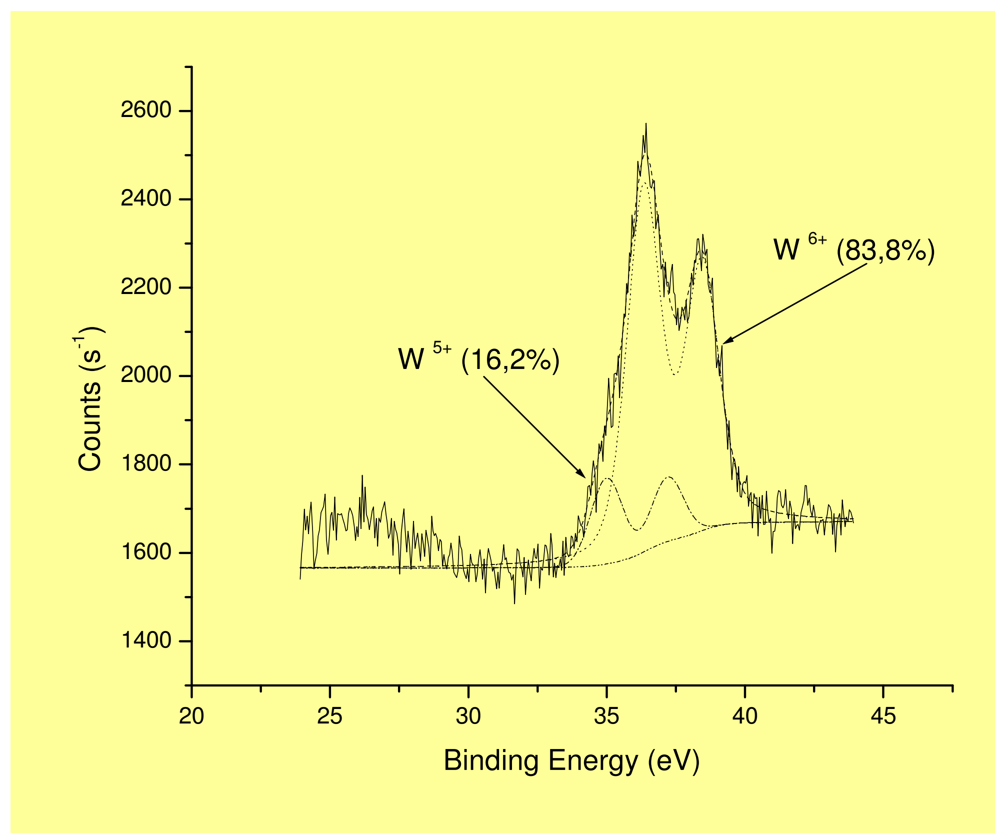

Souza, A.L.; MSc Thesis., IQSC/USP

Adsorção de O_2 e Corrosão sobre Al

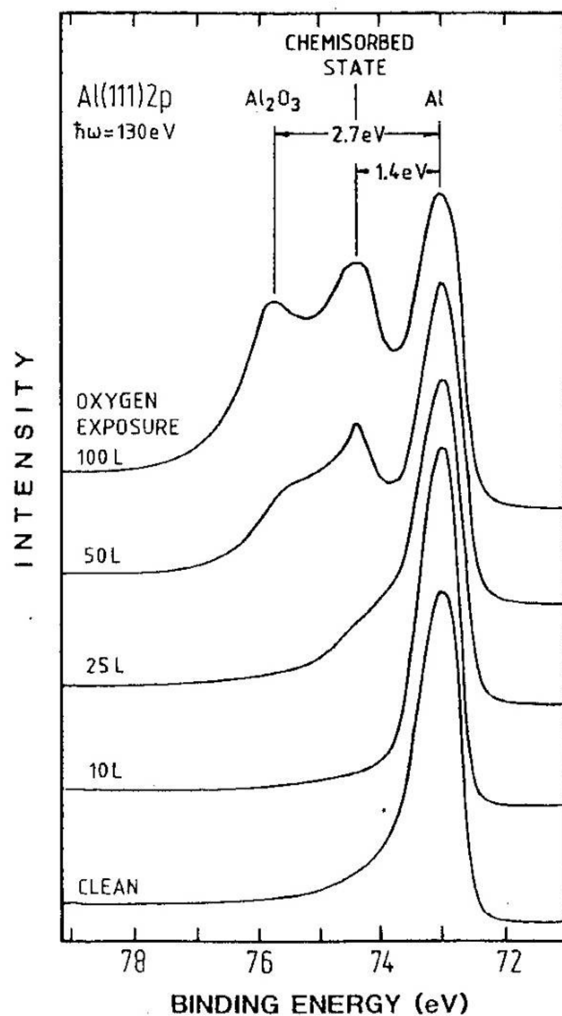

Fig.2.33. Oxidation of a (111) surface of Al monitored via the Al 2p level with $\hbar\omega$ = 130 eV synchrotron radiation [2.75]. The development of a chemisorbed state and subsequent oxide formation can be observed

Análise Semi-Quantitativa

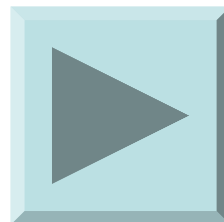

Intensidade da Corrente de Fotoelétrons

Elemento Diferencial de Intensidade

$$dI = FN\sigma\left[\frac{S}{S.sen\theta}\right].\left[-\frac{d}{\lambda.sen\theta}\right].T$$

F = fluxo de fótons

N = concentração do elemento a ser ionizado no material dentro da espessura d

S = área da amostra observada pelo analisador

T = fator de transmissão dado pelas lentes, pelo analisador e dependente da E_c e da E^0

θ = ângulo de coleta = ângulo entre a linha colinear com o analisador e a superfície da amostra

d = profundidade de análise = espessura da camada analisada na amostra

λ = livre percurso médio dos fotoelétrons na amostra

F.S = K para um mesmo equipamento

$$\therefore dI = KN\sigma\left[\frac{1}{S.sen\theta}\right].\left[-\frac{d}{\lambda.sen\theta}\right].T$$

Livre Percurso Médio

Materiais Elementares

$$\lambda = a\left[538.E_c^{-2} + 0.41\sqrt{(aE_c)}\right]$$

E_c dado em eV

a = espessura de uma monocamada

Materiais Inorgânicos

$$\lambda = a\left[2170.E_c^{-2} + 0.72\sqrt{(aE_c)}\right]$$

Materiais Orgânicos

$$\lambda = a\left[\frac{49.E_c^{-2} + 0.11\sqrt{(aE_c)}}{\rho(g.cm^{-3})}\right]$$

Intensidade dos Fotoelétrons

$$I_0 = K.\sigma.N.T.\lambda$$

$$I_d = I_0.\left[1 - e^{-\frac{d}{\lambda.sen\theta}}\right]$$

$$\frac{I_d}{I_0} = \left[1 - e^{-\frac{d}{\lambda.sen\theta}}\right]$$

Sensibilidade XPS

- A sensibilidade da técnica depende da probabilidade de fotoemissão que é dada por:

$$\sigma_{i,j} = A(BE_i\ KE_j) \cdot \left| \left\langle \Psi_i \middle| \mu \middle| \Psi_f \right\rangle \right|^2$$

Momento de transição dipolar elétrico.

- seção de choque (σ)

Seção de Choque para Al κα

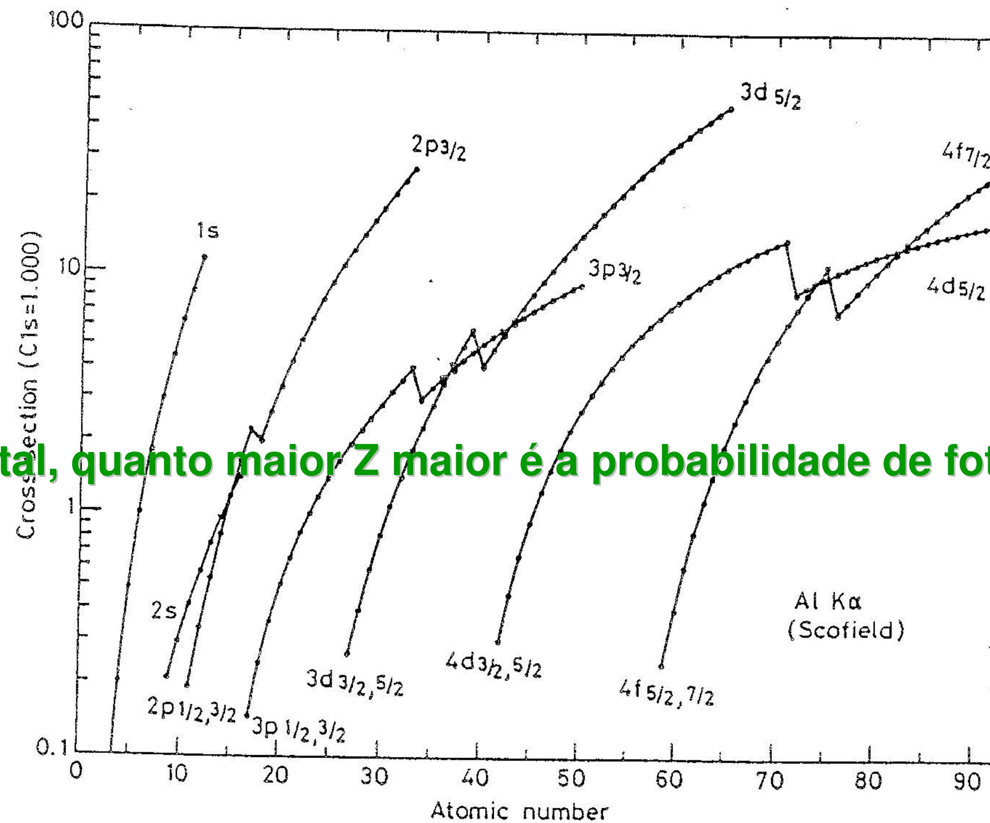

Para um mesmo orbital, quanto maior Z maior é a probabilidade de fotoionização.

Figure 2.20 Calculated values of the cross-section (σ) for Al $K\alpha$ radiation normalised to σ(C1s)=1 (Seah (1990) using original data from Schofield (1976)).

Mínimo de Cooper
Dependência de σ com $h\nu$

Minimum in $\sigma_{i,j}$ about 50 eV (KE) above ionization threshold

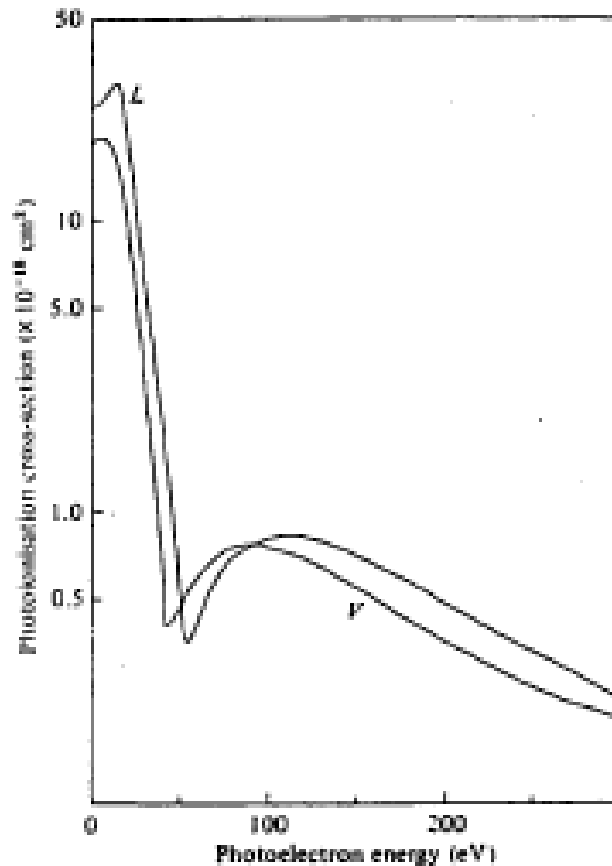

Fig. 3.22 Theoretical computation of the Ar 3p atomic photoionisation cross-section by Kennedy and Manson (1972) showing the 'Cooper minimum' around 50 eV above threshold. *L* and *V* correspond to the 'length' and 'velocity' forms of the matrix element used in the computation (cf. equation (3.12)). These computations include both d and s final states so that the minimum is not identically zero as it is in the d channel alone.

Mínimo de Cooper

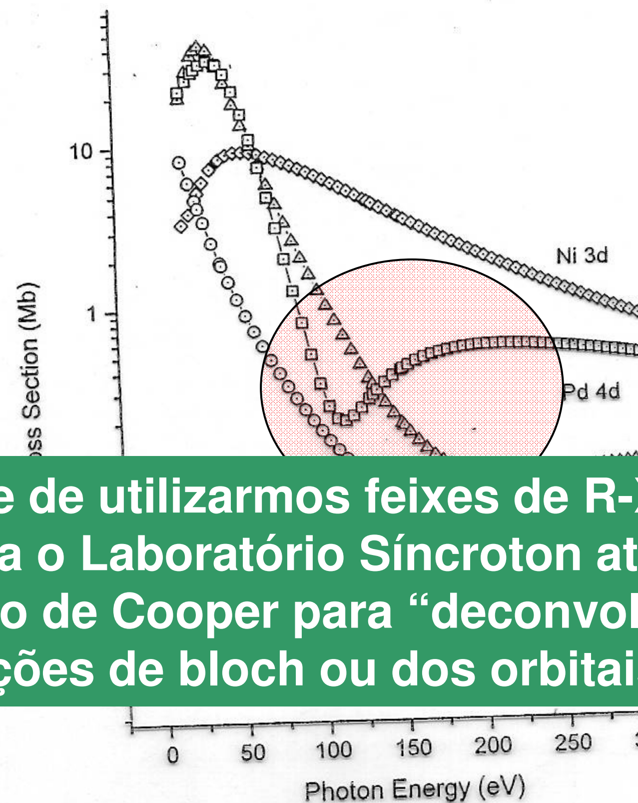

A possibilidade de utilizarmos feixes de R-X com energias diferentes torna o Laboratório Síncroton atrativo, pois podemos nos valer do mínimo de Cooper para “deconvoluir picos ou estudar a COOP das funções de bloch ou dos orbitais moleculares.

Figure 3. Photoionization cross section for the C $2p$, Ni $3d$, Pd $4d$, and Pt $5d$ orbitals.[11]

Resumo

Sensibilidade

Calculations indicate maximum $\sigma_{i,j}$ is ~ 10^{-18} cm^2

If 1 ML contains 10^{15} atoms·cm^{-2}, should get about 10^{-3} photoelectron per incident photons ($10^{15} \times 10^{-18}$)

If x-ray source flux is 10^{12} photons·s^{-1}, should produce about 10^9 electrons·s^{-1} from 1 ML

For most elements, sensitivity is 0.1-1 % ML (≡ subnanomolar)

Observations:

$\sigma_{i,j}$ for C in CF_4, CH_4, graphite… is identical

Each subshell has different $\sigma_{i,j}$ - different sensitivity

Low Z elements have low $\sigma_{i,j}$ implies lower sensitivity

Análise Quantitativa

Difficult to apply calculated $\sigma_{i,j}$ directly to data (other instrumental parameters need to be included)

$$I_a = \Phi_{x-ray}(x,y) \times C_a(x,y,d) \times \sigma_{i,j}(h\nu) \times P_{no-loss}(\text{material},d) \times A_{analyzer} \times T_{analyzer}$$

$\Phi_{x\text{-}ray}$ = x-ray flux

C_a = concentration of element a

$\sigma_{i,j}$ = subshell ionization cross-section

$P_{no\text{-}loss}$ = probability of no-loss escape (α IMFP)

$A_{analyzer}$ = angular acceptance of analyzer

$T_{analyzer}$ - transmission function of analyzer

Fator de Sensibilidade Atômica

Most analyses use empirical calibration constants (called *atomic sensi factors*) derived from standards:

$$C_a(\bar{x},\bar{y},\bar{d}) = \frac{I_{measured}}{ASF}$$

Z	Element	Subshell	ASF (Area)
3	Li	1s	0.012
4	Be	1s	0.039
5	B	1s	0.088
6	C	1s	0.205
7	N	1s	0.38
8	O	1s	0.63
9	F	1s	1.00
10	Ne	1s	1.54
11	Na	1s	2.51
12	Mg	1s	3.65
	Mg	2p	0.07
13	Al	2p	0.11
14	Si	2p	0.17
15	P	2p	0.25

Exatidão < 15%
Usando padrões <5%
Precisão 1%

Importância da Escolha da linha de Base para Quantificação

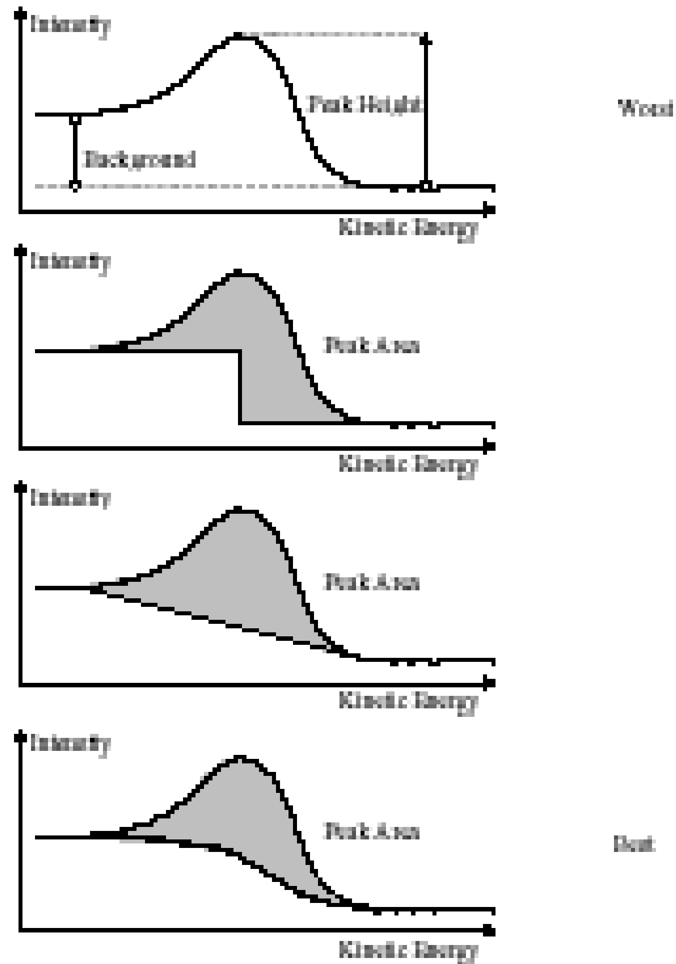

Análise Química Semiquantitativa em Perfil

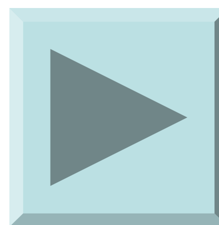

Intensidade da Fotocorrente
Dependência do ângulo de coleta

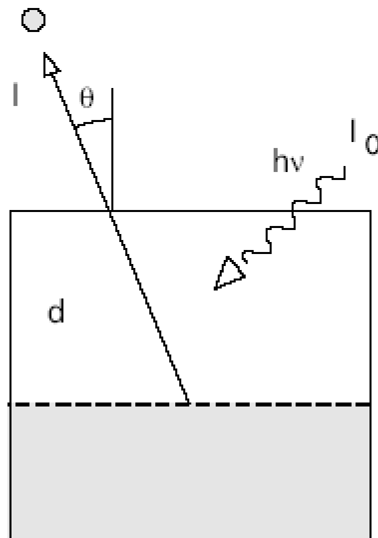

$$I = I_0 \exp\left(\frac{-d}{\lambda \cos\theta}\right)$$

$$\ln\left(\frac{I}{I_0}\right) = \frac{-d}{\lambda \cos\theta}$$

For normal takeoff angle, $\cos\theta = 1$

When $d = \lambda$, $-\ln(I/I_0) = 0.367$ or 63.3 % of electrons come from within 1 λ of surface

When $d = 2\lambda$, $-\ln(I/I_0) = 0.136$ or 86.4 % of electrons come from within 2 λ of surface

When $d = 3\lambda$, $-\ln(I/I_0) = 0.050$ or 95.0 % of electrons come from within 3 λ of surface

Depth profile

Variando o ângulo de coleta

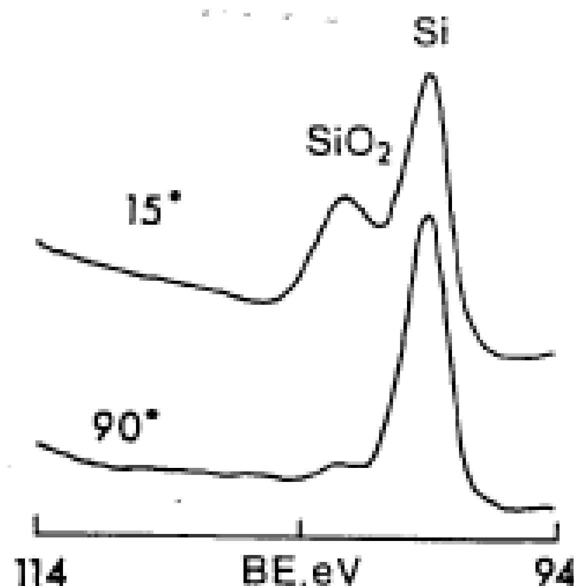

Figure 3.37 Effect of variation of take-off angle on the Si 2*p* spectrum from silicon with a passive oxide layer. Note the relative enhancement of the (surface) oxide signal at low angle (measured with respect to the surface). (After Wagner *et al.*[31])

For off-normal *take-off angle* α:

$$P = \exp\left(\frac{-d}{\lambda \cdot \sin\alpha}\right) \qquad P = \frac{I}{I_0}$$

$$d = -\ln(P) \cdot \lambda \cdot \sin\alpha$$

$$= 3 \cdot \lambda \cdot \sin\alpha$$

d decreases by a factor of 4 on going from $\alpha = 90°$ (normal) to $15°$ (grazing)

Depth Profile

Variando o Ângulo de Coleta

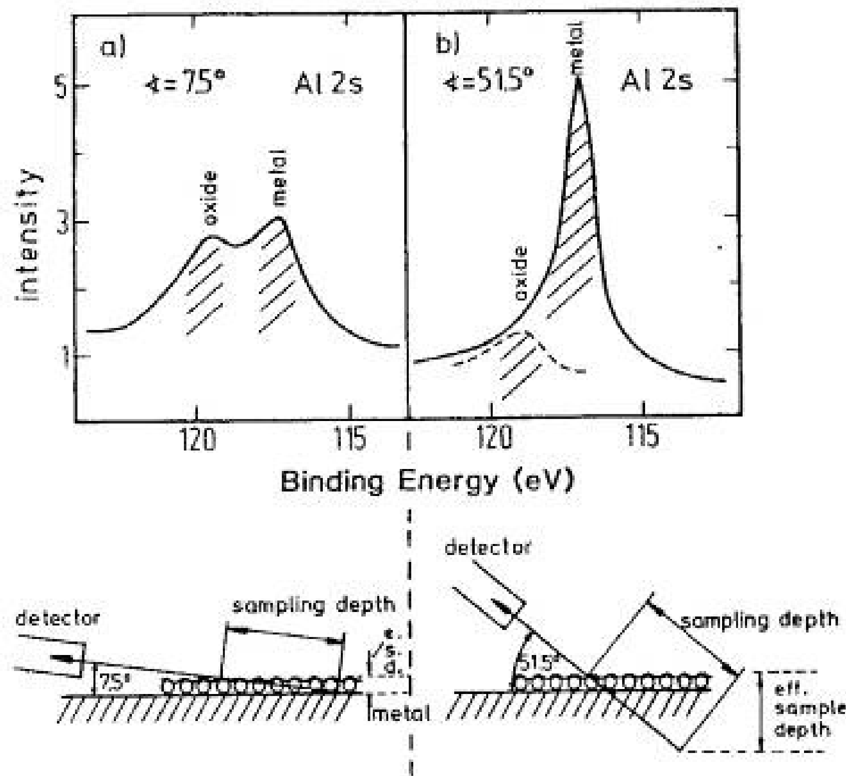

Fig.2.32. Surface sensitivity of XPS, demonstrated by changing the electron detection angle relative to the surface for a slightly oxidized surface of Al. At 7.5°, the Al 2s signals from Al metal and oxidized Al have the same magnitude, while at 51.5° the oxide signal is hardly visible [2.74]

Ion Sputtering
Erosão por Íons Argônio

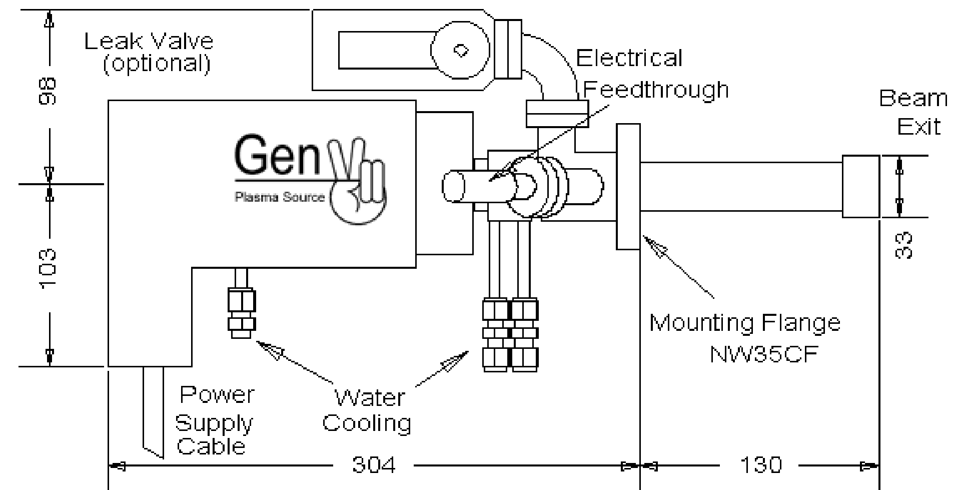

25-5keV, 1mA

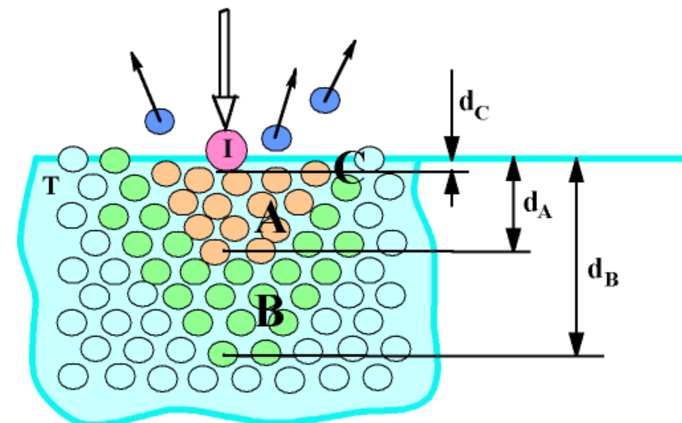

V(nm/s) = 0.104 S (M/d) J cosα
Taxa de erosão= V
S= eficiência de erosão
J= densidade de corrente (mA cm^{-2})
α= ângulo de incidência do feixe de íons

Depth Profile
Sputtering

XPS depth profile of SiO_2 on Si

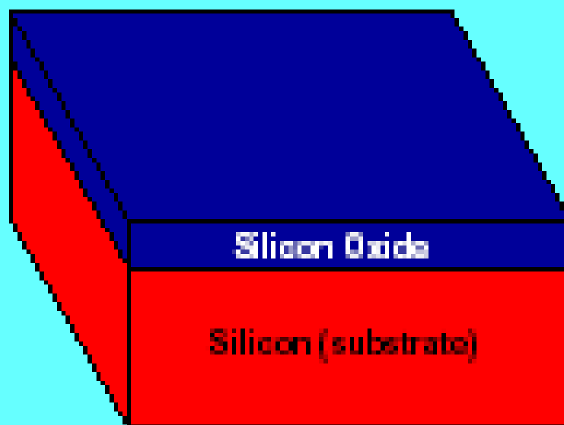

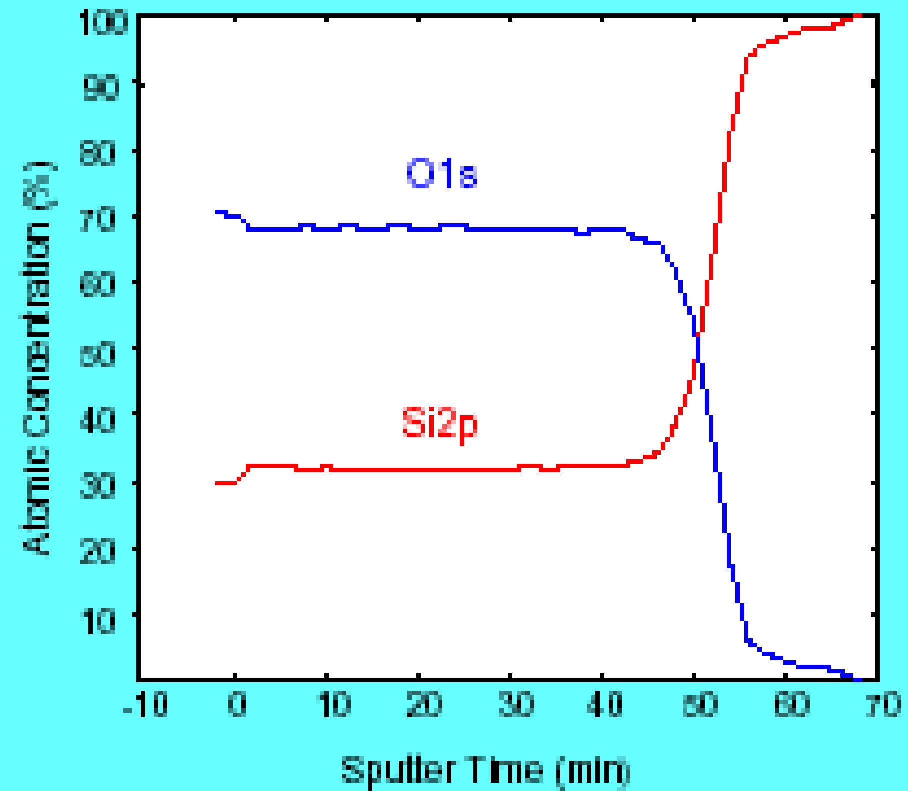

Depth Profile
Sputtering

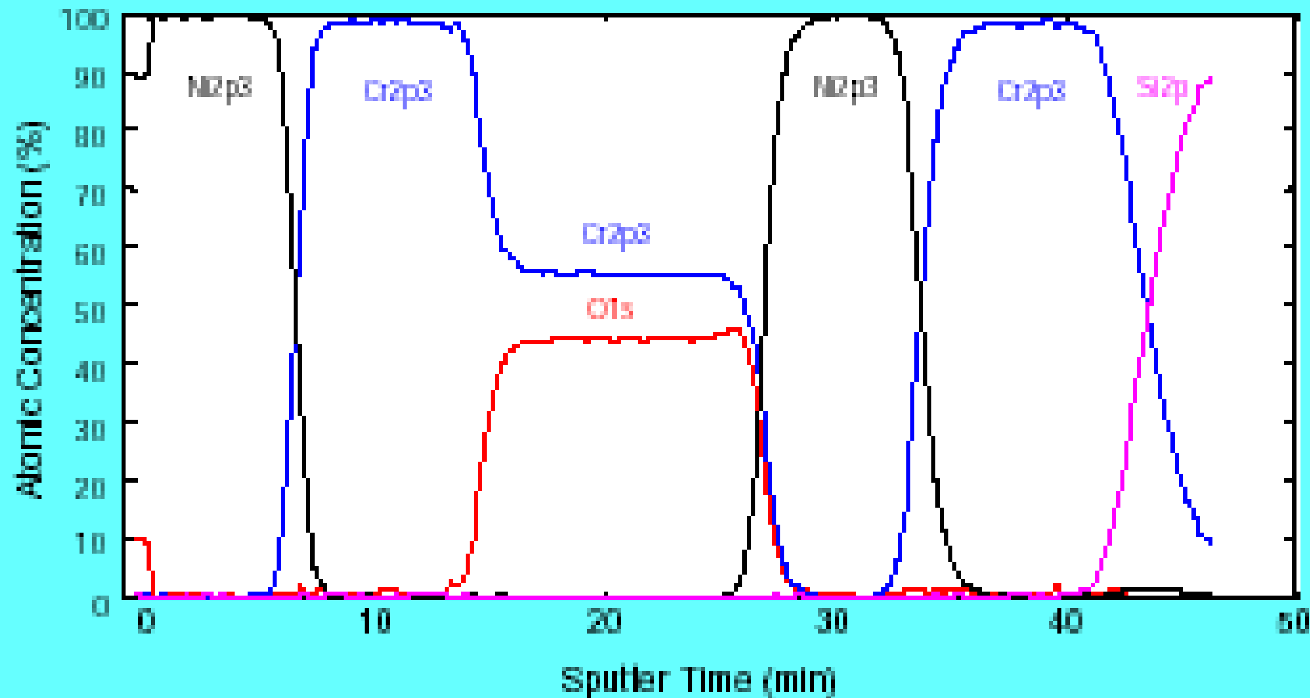

Filmes Anti-corrosivos

Preparation of a self-assembled monolayer on iron by the formation of a covalent bond between carbon and iron atoms

Tadashi Shimura *, Kunitsugu Aramaki

p-Toluenediazonium tetrafluoroborate $CH_3C_6H_4N_2BF_4$ (TDFB)

Formação do Filme por Eletrodeposição

$$[M] + XC_6H_4N_2^+ + e^- \rightarrow [M] - C_6H_4X + N_2$$

Medidas de XPS

X-ray photoelectron spectra of components, Fe 2p, O 1s, C 1s and/or S2p for the disk surfaces modified with TDFB or TT were recorded on an X-ray photoelectron spectrometer with MgK_α radiation as the X-ray source. Depth profiles of the components on the disk surfaces were measured by Ar^+ bombardment of the surfaces with an Ar^+ gun.

Filmes Anti-corrosivos

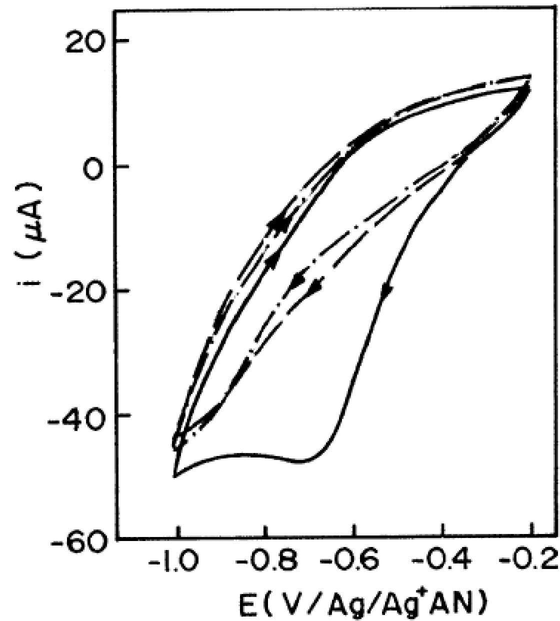

CV durante a deposição a partir de solução em acetonitrila.

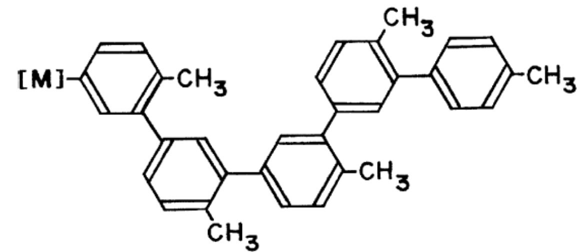

Modelo da estrutura química do filme

Filmes Anti-corrosivos
Eficácia

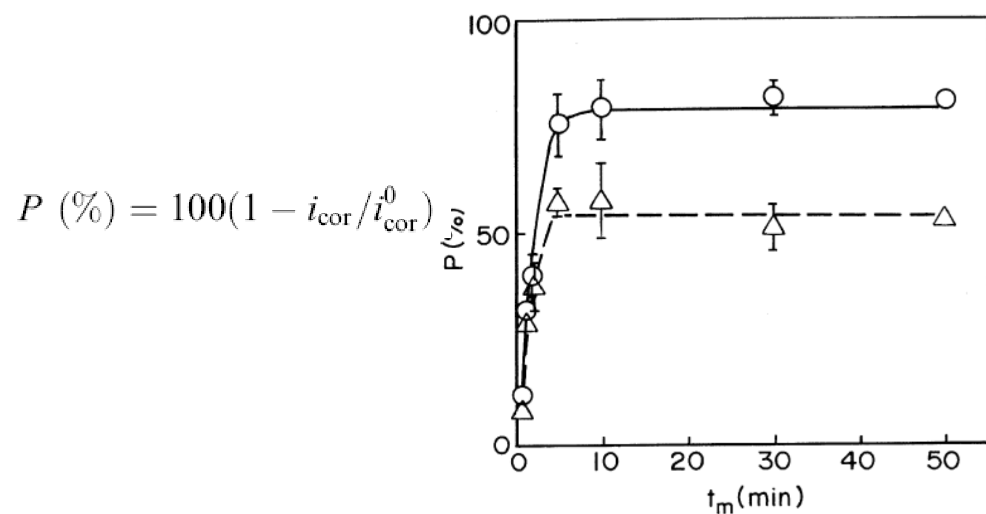

Fig. 5. The values of the protective efficiency, P for the layers prepared by the modification of iron electrode in the TDFB solution after immersion in 0.5 M NaCl for 1.5 (○) and 4.0 h (△) as a function of the modification time, t_m.

$$Fe \rightarrow Fe^{2+} + 2e^-$$

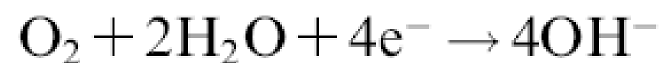

$$O_2 + 2H_2O + 4e^- \rightarrow 4OH^-$$

Filmes Anti-Corrosivos

Depth Profile

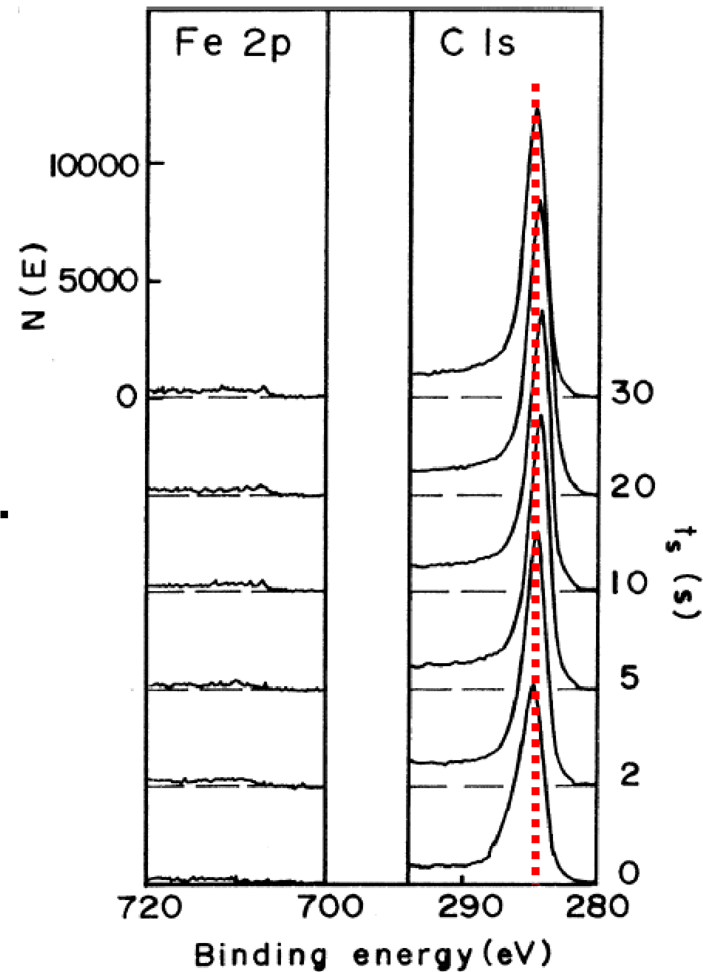

Tempo de deposição 10min.

Da forma apresentada pouca informação pode ser retirada dos dados, o que podemos fazer para extrair mais informação?